JOÃO PEDRO SANTOS PARENTE DA SILVA

ACOUSTIC METHODS FOR ASSESSMENT OF BUBBLES PRODUCED BY MARINE PLANTS

.

Mestrado em Engenharia Elétrica e Eletrónica
Especialidade em Tecnologias de Informação e Telecomunicações

Trabalho efetuado sob a orientação de:
Professor Doutor Paulo Felisberto
Professor Doutor António Silva

UNIVERSIDADE DO ALGARVE
Instituto Superior de Engenharia
2018

ACOUSTIC METHODS FOR ASSESSMENT OF BUBBLES PRODUCED BY MARINE PLANTS

Declaração de autoria de trabalho

Declaro ser o autor deste trabalho, que é original e inédito. Autores e trabalhos consultados estão devidamente citados no texto e constam da listagem de referências incluída.

I hereby declare to be the author of this work, which is original and unpublished. Authors and works consulted are properly cited in the text and included in the reference list.

João Pedro Santos Parente da Silva

(João Pedro Santos Parente da Silva)

Resumo

A propagação acústica no oceano é fortemente influenciada pela ocorrência de bolhas na coluna de água, sendo essas bolhas resultado de vários processos que ocorrem no oceano. Um desses processos é a formação e subsequente libertação de bolhas de oxigénio produzidas pelas ervas marinhas durante o processo de fotossíntese.

Esta dissertação de mestrado visa avaliar diferentes métodos acústicos de caracterização de bolhas de ar e fazer o estudo da sua aplicação à estimação das bolhas de oxigénio. Atualmente, existem vários métodos descritos na literatura para estimar a quantidade e a distribuição de bolhas de ar em ambientes aquáticos. No entanto, esses métodos visam essencialmente a sua aplicação no estudo das bolhas existentes na superfície do oceano provocadas pela agitação marítima. Em certas condições, o oxigénio libertado pelas plantas marinhas durante o processo de fotossíntese ocorre sobre a forma de bolhas de oxigénio. A quantificação desta componente da produção das plantas é difícil de ser feita e considera-se que muitas vezes é subestimada pelos métodos usualmente utilizados. Os métodos acústicos são bastante úteis neste caso pois podem ser potencialmente utilizados para fazer a estimação da produção de bolhas com mais exatidão, e, para além disso, permitem perceber a dinâmica desta produção de bolhas pelas plantas marinhas.

Assim, inicialmente foi feita uma avaliação do processo de libertação de bolhas das plantas para a coluna de água, do modelo da propagação acústica numa zona

com ervas marinhas e da configuração de todo o sistema. Foram também avaliados e tidos em consideração a presença de vários parâmetros indesejados no sinal recebido (por exemplo, mudanças de temperatura, ruído, maré, velocidade do som na água, salinidade) e feita uma caracterização do ruído ambiental e biológico.

Neste trabalho, propõe-se avaliar métodos genéricos de estimação de bolhas descritos na literatura e fazer a sua adaptação no desenvolvimento de novos métodos para fazer a monitorização da libertação de bolhas produzidas pelas plantas marinhas, mais concretamente utilizando o método de medição dos tempos de propagação e no caso particular de uma planta muito abundante na *Ria Formosa*, a *Cymodocea nodosa*. Através da combinação de métodos acústicos com outros métodos convencionais, tornou-se possível o desenvolvimento de um sistema de medição acústico preciso e robusto para fazer a geração e aquisição dos sinais acústicos. Estes sinais acústicos após serem adquiridos são então processados através da ajuda de um software interativo de alta performance, *Matlab*, para posteriormente ser feita a estimação da quantidade de bolhas de oxigénio produzidas num determinado ambiente marinho. O desenvolvimento deste sistema de medição acústico pode vir a ser uma grande ajuda para o estudo dos ecossistemas marinhos, pois acredito que este inovador método acústico pode ajudar no estudo do metabolismo de um determinado ecossistema, e que por isso, virá a tornar-se uma ferramenta bastante útil para ser feita a monitorização e controlo da produção de áreas costeiras integrando escalas espaciais e temporais.

Palavras chave: processamento de sinal, sistema de medição acústico, bolhas subaquáticas, oceanografia acústica, produção de oxigénio, bolhas de oxigénio, ervas marinhas

Abstract

The aim of this dissertation is to evaluate different acoustic methods to characterise air bubbles and their application in the estimation of oxygen bubbles produced by marine plants during the photosynthesis process. Several methods are described in the literature to estimate the amount and distribution of air bubbles in marine waters however, the existing methods focus essentially on bubbles at the ocean's surface. Under certain conditions, the oxygen released by marine plants during photosynthesis occurs in the form of bubbles. The estimation of this bubbles is difficult and is often considered underestimated by conventional methods. Acoustic methods can be used to estimate the production of bubbles with greater precision and, moreover, to learn the dynamics of their production.

It is necessary to evaluate the oxygen transfer process of the plants to the water, the model of acoustic propagation in seagrass fields, the configuration of the system, methods to filter the influence of unwanted parameters on the received signal (e.g., temperature changes, noise, tide, sound speed, salinity), and, to characterise environmental and biological noise.

In this work, I propose to evaluate a suitability and generic bubble estimation method described in the literature, or the development of new methods for the monitoring of bubbles released by marine plants, in particular, seagrass *Cymodocea Nodosa*. The reliability of a generic bubble estimation method described in the literature,

as well as, new methods for monitoring the bubbles released by marine plants will be tested. All the tests were conducted with the *Cymodocea Nodosa* seagrass species, in tanks on IPMA-EPPO. Combining acoustic with other techniques (CTD data, tide height) will allow the development of a robust and accurate acoustic measurement system. The acquired signals can be processed to estimate the amount of oxygen bubbles produced in that environment. With the use of this measurement system, I believe that this innovative acoustic method can be used to accurately quantify the ecosystem metabolism and that it will represent an important tool to manage and monitor the production of coastal areas by integrating spatial and temporal scales.

Keywords: signal processing, acoustic measurements system, underwater bubbles, acoustic oceanography, oxygen production, oxygen bubbles, seagrass meadow

To my grandfather

wherever you are

Acknowledgments

First of all, I want to thank my advisor, *Prof. Dr. Paulo Felisberto* and *Prof. Dr. António Silva*, for all the commitment and dedication with which they have accompanied me in this work, for all their help and availability.

I would like to thank the technical and scientific staff at IPMA-EPPO, in particular to *Hugo Ferreira*, for the logistics, and *Friedrich Zabel* for his precious help in preparation and assembly of the equipment during the various experiments and for the support, knowledge and friendship along of the project.

To my academy friends who accompanied me and supported along this journey, especially to *João "Frieza" Pereira* for their friendship and constant and precious help since Day 1 of our academic journey.

To my friends for all the encouragement and support they gave me to complete this master thesis, specially *Andréa Afonso*, *Daniel Martins* and *Ana Lúcia* who have always been with me since for many years.

I could not fail to thank to my girlfriend, a person who accompanies me every single day of my life. Big part of this thesis it is thanks to her, for all the support when I was down and without motivation. *Paula Silva*, thank you from the bottom of my heart.

Last but definitely not least, to the persons most important of my life, to my parents and sister. All the unconditional support and encouragement they have provided me

over the years was the greatest gift anyone has ever given me. They taught me the value of hardwork and an education. Without them, I may never have gotten to where I am today.

This work was funded by National Funds through Foundation for Science and Technology (FCT) under project PTDC/EEIPRO/2598/2014 (SEAOX).

FCT
Fundação para a Ciência e a Tecnologia
MINISTÉRIO DA CIÊNCIA, TECNOLOGIA E ENSINO SUPERIOR

Table of Contents

List of Tables

List of Figures

List of Abbreviations

ABS	Acoustic Backscatter System
ADC	Analog-to-digital converter
BNC	Bayonet Neill–Concelman connector
CTD	Conductivity, temperature and pressure instrument
CW	Continuous waveform
DAC	Digital-to-analog converter
DC	Direct current
DHCP	Dynamic Host Configuration Protocol
EMI	Electromagnetic interference
EPPO	Aquaculture Research Station in Olhão
INF	Infinite
FCT	Foundation for Science and Technology
FPGA	Field Programmable Gate Array
IP	Internet Protocol
IPMA	Portuguese Institute for the Sea and Atmosphere
LAN	Local area network
MatLab	MATrix LABoratory software
PC	Personal computer
rms	Root mean square

RP	Red Pitaya
SCPI	Standard Commands for Programmable Instrumentation
SD	Secure Digital
SEAOX	Using acoustics for monitoring the metabolism of marine ecosystems project
SL	Source level
SNR	Signal-to-noise ratio
SVP	Sound velocity profiler
TR	Transmitter Receiver
TRR	Transmitter Receiver Receiver
TVR	Transmit voltage response
URL	Uniform Resource Locator
USB	Universal Serial Bus

$C_6H_{12}O_6$	Glucose (sugar)
CO_2	Carbon dioxide
H_2O	Water
O_2	Oxygen

m	Meter
μm	Micrometer
cm	Centimetre
nm	Nanometre
m/s	Meter per second (speed unit)
ms	Millisecond
%	Percentage
Hz	Hertz (frequency unit)
kHz	Kilohertz
MHz	Mega-Hertz

$Mbit$	Mega-Bit
MS/s	Mega-Samples per second
kS/s	Kilo-Samples per second
dB	decibel
V	Volt (electric potential unit)
Ω	Ohm
Ah	Ampere hour (electric charge unit)
nF	Nano-farad
kPa	Kilo-pascal (pressure unit)

List of Symbols

a	Largest active dimension of the source
am	ante merīdiem (before midday)
b	Bubble radius
CL	Load Capacitance
CT	Transducer Capacitance
D	Water depth
c_e	Effective sound speed
c_g	Gas sound speed
c_w	Bubble free water sound speed
f	Frequency
f_0	Bubbles ressonance frequency
h	Distance from the bottom
l_d	Path length of the direct echo
l_b	Path length of the bottom reflected echo
l_s	Path length of the surface reflected echo
N	Number of cycles
RL	Load Resistance
pm	post merīdiem (after midday)
ρ_g	Gas density

ρ_w	Bubble free water density
r	Distance between the sound source and the receiver
τ_d	Travel time of the direct echo
τ_b	Travel time of the bottom reflected echo
τ_s	Travel time of the surface reflected echo
T_w	Total duration of the probe signal
χ	Void fraction
λ	Signal wavelength

1

Introduction

Seagrasses are marine plants that cover large coastal areas worldwide. Seagrass beds are among the most productive ecosystems on earth, providing important amounts of oxygen by photosynthesis. Previous experiments conducted in *Posidonia oceanica* meadow (in STARESO, *Station de Recherches Sous Marines Et Océanographiques* in Calvi, France) have shown a high correlation between the photosynthesis activity assessed by dissolved oxygen sensors and the attenuation of low frequency signals emitted from a controlled source to a distant receiver (source-receiver distances between 50 and 1000 m) ((Felisberto et al., 2015) and references therein). The attenuation of the acoustic signals was mainly ascribed to bubbles formation during photosynthesis, which might be particularly relevant under oxygen supersaturation conditions (dissolved

oxygen above 100 %). While oxygen bubbles have an important impact on acoustic propagation, the dissolved oxygen has not. Since bubbles are difficult to assess by conventional methods commonly used in field measurements, the oxygen production of seagrass ecosystems might be underestimated. Unlike other methods that simply provide local oxygen measurements (water analysis, oxygen probes), acoustic based methods can offer integral information over the propagation paths between the source and the distant receiver by using a single system, thus allowing the monitoring of average oxygen productivity of large coastal areas.

Bubbles in water have a very specific acoustic signature. Several methods have been developed for acoustic characterization of gas bubbles in the seawater (Medwin & Clay, 1998). In seagrass ecosystems, most of the oxygen produced by photosynthesis is released into the water by diffusion, but under oxygen supersaturation conditions, bubbles might be formed at the surface of leaves. The acoustic signature is ascribed to:

- O_2 bubbles released to the water column,
- pressurization of the arenchyma,
- O_2 released to roots and sediments.

The occurrence and strength of the acoustic signature may vary among seagrass species and environmental conditions. The signature is also frequency dependent. During photosynthesis the pressurisation of plants aerenchyma occurs, as the oxygen produced diffuses into it (Borum et al., 2006). Internal pressurisation of 15kPa above atmospheric pressure has been reported for *Cymodocea nodosa* under the light, whereas in the dark it decreased to values below the partial pressure of air in seawater. The pressurisation can also lead to bubble formation at the leaf tips, particularly if these are damaged. Aerenchyma pressurisation, and particularly bubbles have an acoustic signature, therefore acoustic based methods may offer an important contribution to the monitoring of seagrass ecosystems.

More recently, acoustic experiments performed in the framework of SEAOX project in a pond covered by the *Cymodocea nodosa* and *Zostera marina* , using low frequency signals (ambient noise and controlled sources) propagating through the meadow and a high frequency backscatter device, corroborate earlier findings of a significant release of bubbles by photosynthesis in oxygen supersaturation conditions (Felisberto et al., 2017b). Preliminary results of gas bubbles void fraction estimates (fraction of air bubbles to the volume of water) were obtained independently from ambient noise data and from low frequency controlled signals. Both methods estimated gas void fraction as high as 10^{-4}. However, the experiment also shows the need for an acoustic system that measures the bubbles production at short distances (plants level) to avoid the influence of the water depth variability due to tide. The system implemented in this master thesis will be based on precise measurements of travel time and signal attenuation, therefore the sound source and the receiver will be accurately synchronized. Such a system will provide accurate results and will serve as a baseline for the calibration of bubbles quantification methods at the pond level.

1.1 Scope of the Thesis

This master thesis is integrated in the project SEAOX: Using acoustics for monitoring the metabolism of marine ecosystems, funded by National Funds through Portuguese Foundation for Science and Technology (FCT) under project PTDC/EEIPRO/2598/2014. The project started in June, 2016 and lasts for three years.

In summary, the project aims to use the properties of sound propagation in ocean water as a proxy of the amount of oxygen bubbles to monitor the photosynthetic production of marine plants at various spatial and temporal scales. The work presented in this thesis focus on the study and development of an acoustic measurement system using the method of travel time measurement to estimate the oxygen bubble production of marine plants at plant scale (short range local measurements).

1.2 Objectives

As mentioned above, the main objective of this thesis is to develop a measurement system using the properties of underwater acoustics signals propagation to characterize and quantify the oxygen bubbles produced by marine plants during the photosynthesis.

As such, the objectives of this master's thesis are to carry out several specific steps, each having a defined objective. The steps are as follows:

1. **State of the art**

   The objective of this step is to make state of the art about methods of measurement of bubbles in the water column and learn more about acoustic underwater. This is a very important stage of this work because underwater acoustic is a new theme for the thesis author. The objective is to do an initial theoretical and practical study of the theme.

2. **Development measurement system**

   The purpose of this assignment is to develop the innovative and accurate measurement system to generate and acquire underwater acoustic signals, develop and deliver accurate travel time and signal attenuation measurements to the estimation methods to quantify oxygen bubbles produced by a seagrass meadow.

3. **Calibration and verification**

   The objective of this step is to calibrate the whole system through the execution of several experiments in tanks with controlled conditions.

4. **Final validation test**

   The last step is to perform the final experiment of the entire calibrated system. The objective is to execute this experiment in a tank in a *Ria Formosa* lagoon.

1.3 Overview of the Thesis

This document focus on practical aspects of the development, calibration and field operation of an acquisition system for the characterization of bubbles released by marine plants. The system is organised as follows.

The current chapter introduced the thesis theme as well as the main goals, shows the whole structure of the document separated by five chapters and contributions and scope of this work.

Chapter 2 provides brief explanation about the biological processes related to the oxygen production of marine plants and bubbles release.

Chapter 3 is about the principles of acoustic detection and quantification of gas bubbles. This chapter presents the background related to bubble characterization using a specified method, travel time measurement using low frequency pulses and attenuation of the signal related to bubble size.

Chapter 4 presents the measurement system developed to generate and acquire acoustic signals to estimate oxygen bubbles production. The components used in this system are specified in detail in this chapter. Also presents calibration of the system through the execution of several experiments.

Chapter 5 presents the field experiments to test the calibrated measurement system. Also in this chapter, provides other tank experiments realized during all project.

Chapter 6 is the final chapter, concluding this thesis and all work done in previous chapters along with the future work and publications accomplished over the project.

In the appendices, additional documents are provided to better explain the operation of the system and its development.

2

Biological phenomena

Algae and marine plants are largely responsible for most of the oxygen production on Earth. For oxygen to be produced by marine plants, a series of biological phenomena must occur in order for plants to produce and release oxygen into the water column.

These phenomena are extremely important for the sustainability of the marine ecosystem since the production of oxygen is essential for the survival of all living organisms.

2.1 Photosynthesis process

Photosynthesis is the amazing chemical process by which organisms use sunlight, carbon dioxide and water to create the energy they need to live. While most people think that photosynthesis is conducted by green plants living on the ground, it is achieved by a variety of bacteria, algae, and underwater plants. Photosynthesis is largely responsible for producing and maintaining the oxygen content of the Earth's atmosphere and supplies all of the organic compounds and most of the energy necessary for life on Earth (Wetzel, 2001; Todar, 2012).

Plants, algae, as well as cyanobacteria, are responsible for a major part of photosynthesis in oceans because they have plenty of water to work with, so their main challenge is getting enough sunlight and air. These organisms convert CO_2 (carbon dioxide) to organic material by reducing this gas to carbohydrates in a rather complex set of reactions. Electrons for this reduction reaction ultimately come from water, which is then converted to oxygen and protons (Watt, 2000).

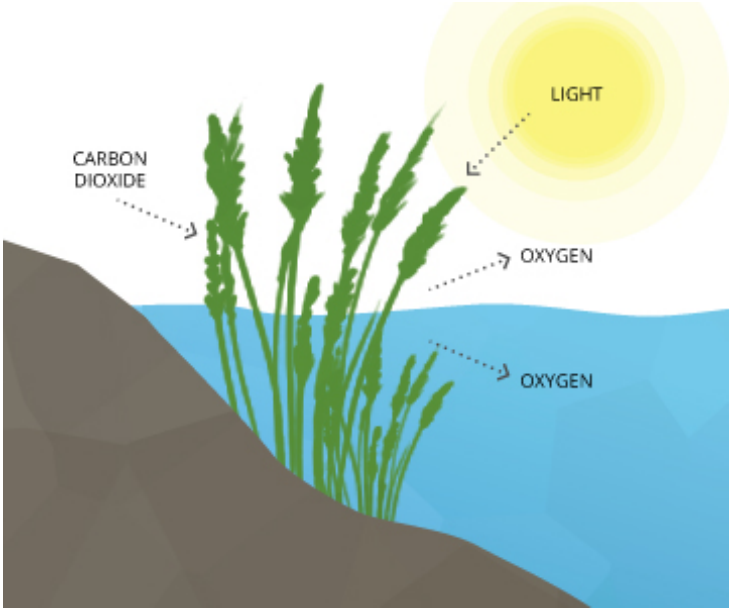

Figure 2.1: Photosynthesis process. Basically, photosynthesis uses water, carbon dioxide and sunlight to produce energy and oxygen (Scales, 2009).

The overall balanced chemical equation for the photosynthesis reaction is:

$$6\,CO_2 + 6\,H_2O \xrightarrow{sunlight} C_6H_{12}O_6 + 6\,O_2 \tag{2.1}$$

Where:

$$[CO_2] \Rightarrow \text{Carbon dioxide}$$

$$[H_2O] \Rightarrow \text{Water}$$

$$[C_6H_{12}O_6] \Rightarrow \text{Glucose (sugar)}$$

$$[O_2] \Rightarrow \text{Oxygen}$$

In most plants, photosynthesis occurs in special cells known as chloroplasts. The green hue we see in plants is the result of tiny grains of green pigment (light-absorbing molecules) inside the chloroplasts. These pigments are commonly known as chlorophyll (chloro is related to green and phyll is related to leaf).

Energy for this process is provided by light, which is absorbed by pigments (primarily chlorophylls and carotenoids). The light energy required by photosynthesis process optimally occurs in the 400 to 700 nm range and is also known as visible light (Wetzel, 2001).

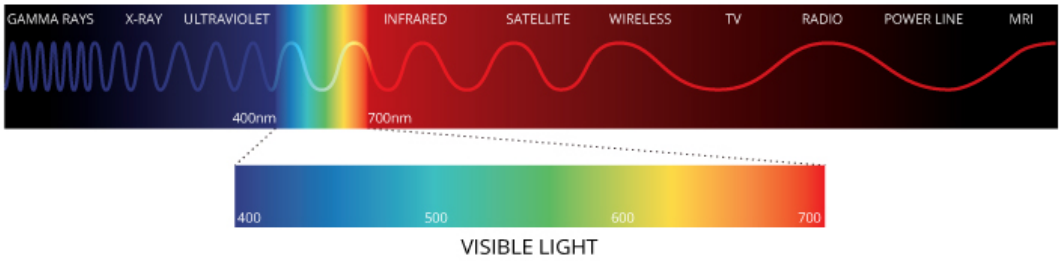

Figure 2.2: Visible light range that occurs light absorption by plants (Fondriest Environmental, 2014).

Chlorophylls absorb blue and red light and carotenoids absorb blue-green light, but green and yellow light are not effectively absorbed by photosynthetic pigments in plants. Therefore, light of these colours is either reflected by leaves or passes through the leaves and this is the explain to the green colour of plants (Netting, 2007), as shown in Figure 2.3

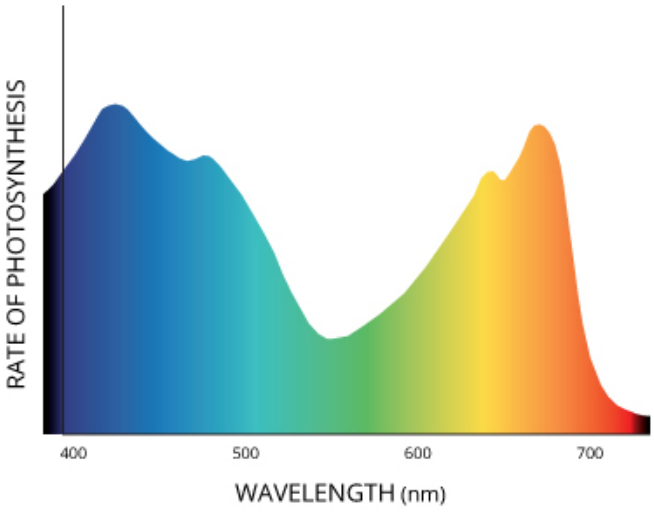

Figure 2.3: Relation between wavelength and rate of photosynthesis (Fondriest Environmental, 2014).

Underwater plants still need sunlight to perform photosynthesis, but fortunately, sunlight can pass through the water easily enough. This is why many aquatic plans may have stems that reach down hundreds of feet, but most of the plant floats near the surface, where it can absorb the sunlight. Aquatic plants are also usually green like topside plants, to absorb the most of the sunlight spectrum that enters the atmosphere. Photosynthesis can occur as long as enough light is available for the chlorophyll and other pigments to absorb. In the ocean, light can reach as far as 200m below the surface (Television, 2014). This zone is known as the euphotic zone or sunlight zone, as shown in Figure 2.4. Only a small amount of light penetrates beyond this depth, but it's not

enough for photosynthesis to occur (Oceanic & Administration, 2013).

However, the sunlight that enters the water is affected by more variables. Not only do aquatic plants have to deal with cloudy days, but also with cloudy water. Silt and mud stirred up in active water can create a barrier between plants and sunlight. The colour of the water, which is affected by plankton and minerals, can also have an effect on how much sunlight can make it through to the plants.

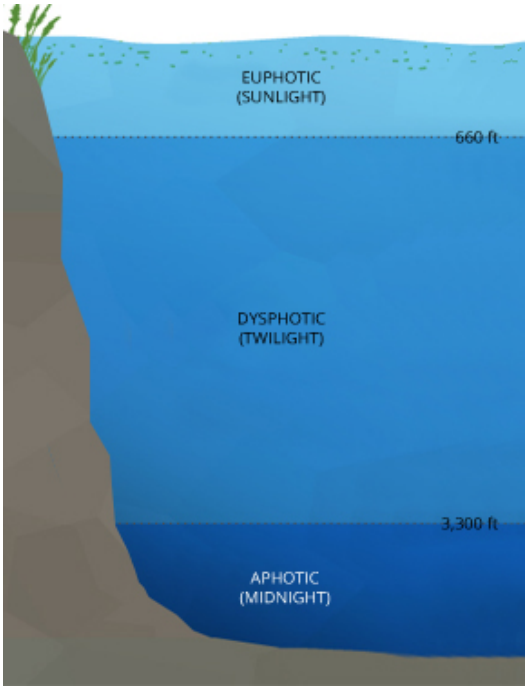

Figure 2.4: Water column of the ocean (Fondriest Environmental, 2014).

During a sunny day, dissolved oxygen in water is generally plentiful because photosynthesising algae and aquatic plants are constantly releasing it into the water. Even though many other organisms are using the oxygen, there is an oxygen surplus.

After sundown, without sunlight, photosynthesis slows considerably or even stops. So, in addition to the usual oxygen demands (from fish, macro-invertebrates, tadpoles, etc.), algae and plants are also pulling oxygen from the water.

Factors that influence the rate of photosynthesis and oxygen production in marine plants are:

- **Temperature**

  Photosynthesis requires heat to active the process. In addition, higher temperatures can also speed up chemical reactions. Although increased temperatures can speed up photosynthesis, too much heat can be detrimental (Barber, 2014). At a certain temperature, enzymes become denatured, lose their shapes and no longer speed up chemical reactions. Above the optimum temperature the rate of photosynthesis begins to decrease, until it stops (see Figure 2.5).

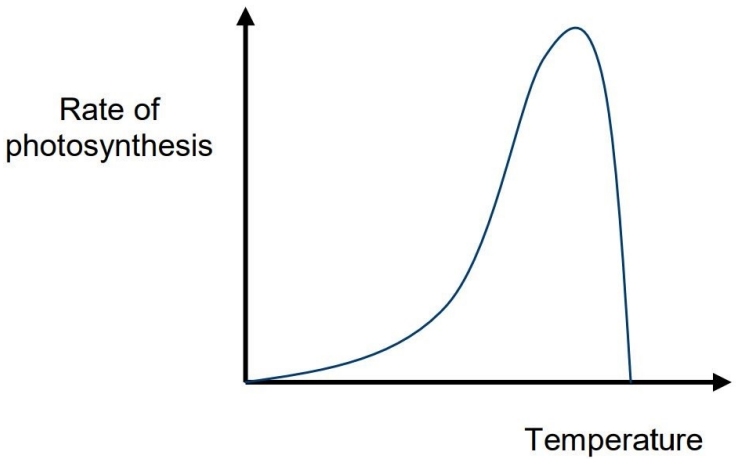

Figure 2.5: Relation between the temperature and rate of photosynthesis (Royal Society of Chemistry, 2012).

- **Carbon dioxide concentration**

  An increase in the carbon dioxide concentration increases the rate at which carbon is incorporated into carbohydrate in the light-independent reaction (Silverstein, 2008), and so the rate of photosynthesis generally increases until limited by

another factor. As it is normally present in the atmosphere at very low concentrations (about 0.04%), increasing carbon dioxide concentration causes a rapid rise in the rate of photosynthesis, which eventually establish when the maximum rate of fixation is reached. This phenomenon can be seen in the Figure 2.6.

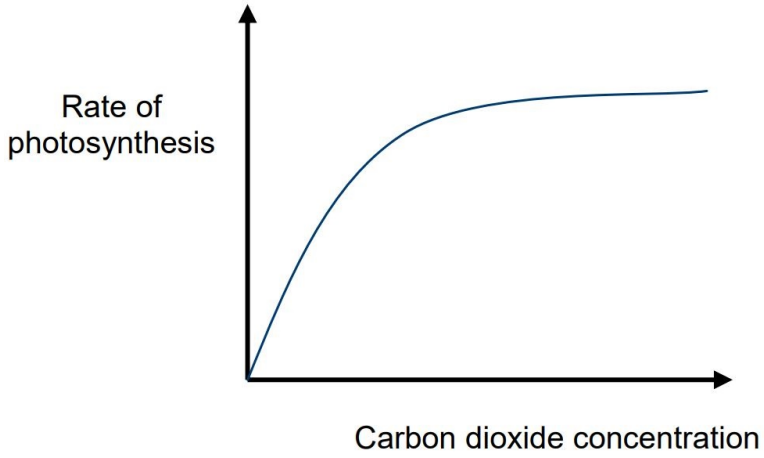

Figure 2.6: Relation between the carbon dioxide concentration and rate of photosynthesis (Royal Society of Chemistry, 2012).

- **Water colour**

  Dissolved substances in the water, such as naturally-occurring tea-coloured tannins, can prevent sunlight from penetrating down into the water column. This is one reason that many red-water or black-water lakes have few submersed plants. There isn't enough light to allow photosynthesis below a certain depth. These lakes can support emersed or floating-leaved plants which are in direct contact with the sunlight.

- **Turbidity**

  Turbidity is a lack of water clarity caused by the presence of particles (Wetzel, 2001). These particles can be clay, silt or free-floating algae. The big problem

is that these particles absorb sunlight and can cause light to be reflected off the particles in water. The more particles present in the water, the less photosynthetically active radiation that will be received by plants and phytoplankton and consequently decreases the rate of photosynthesis. If the photosynthetic production is restricted, the dissolved oxygen level in the water column will decrease.

- **Cloudy weather**

  Several days of cloudy weather can slow the rate of photosynthesis, resulting in lower oxygen production within a waterbody.

- **Day length**

  Fewer daylight hours (during autumn and winter) also influence photosynthesis, as well as temperature and humidity.

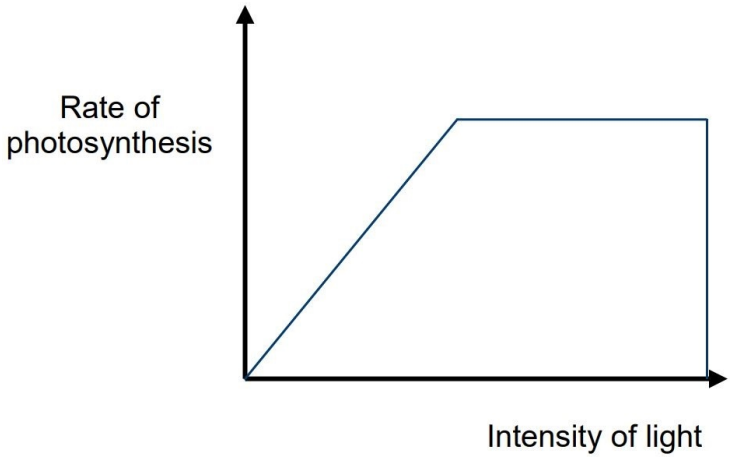

Figure 2.7: Relation between the intensity of light and rate of photosynthesis (Royal Society of Chemistry, 2012).

Water colour, turbidity, cloudy weather and day length are factors related with intensity of light. At low light intensities, as light intensity increases, the rate of

photosynthesis generally, increase proportionately. As light intensity is increased further, however, the rate of photosynthesis is eventually limited by some other factors and establishes at this limit. At very high light intensity, chlorophyll may be damaged and the rate of photosynthesis drops steeply until stops, as shown in Figure 2.7.

- **Leaf characteristics**

  Changes in the condition of a leaf (aging, tearing, etc.), the arrangement of leaves on a branch, even the shape and size of a leaf affects the amount of photosynthesis that occurs in a plant, so much so that two different types of plants have developed over time, based on their tolerance for light.

  Sun plants experience an increased rate of photosynthesis as light intensity increases. Leaves on a sun plant tend to be smaller and thicker, with more pronounced lobes than shade plant leaves (see below). Special cells in these leaves allow higher rates of photosynthesis.

  Shade plants photosynthesise at a lower rate, even if a lot of light is available. Their leaves tend to be thinner and longer, with fewer chlorophyll cells, making it easier to photosynthesise under low light conditions. The marine plants used during the work performed are of this type of plants.

2.2 Pearling

Pearling is a phenomenon that occurs in marine plants that consists of the appearance of small air bubbles in the end of the leaves of the plants. These bubbles gradually increase in size until released by plants to the top of the water column (Okeanos aquascaping, 2013).

The occurrence of this phenomenon is directly related to the overall well-being of the plant, due to the fact that it is a proof that the plant is correctly performing the process of photosynthesis, in this case in an environment of oxygen saturation in the water column.

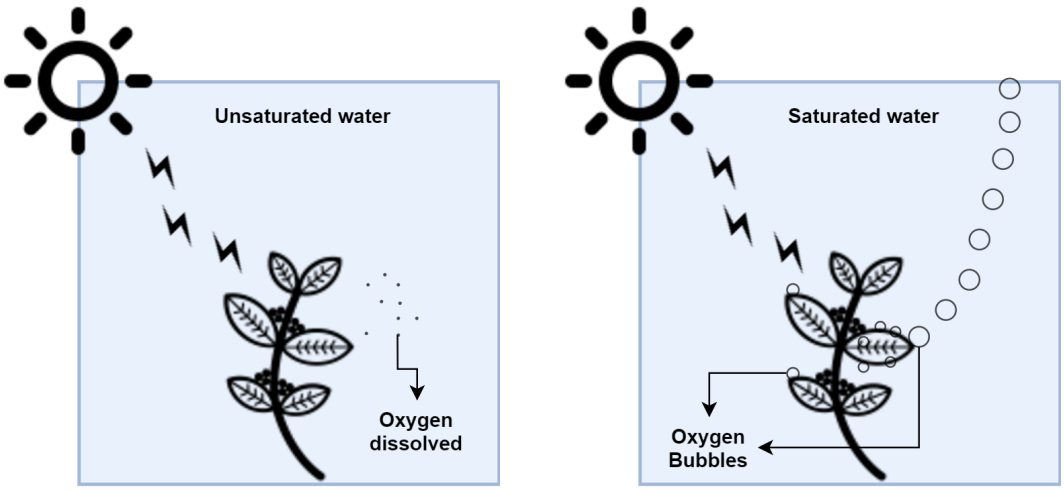

Figure 2.8: Occurrence of oxygen bubble release in the plant leaf. Bubbles do not form and oxygen is dissolved when the water is unsaturated, on the left, and the bubbles are released up to the top of the water column when water is saturated, on the right.

As already mentioned in the previous section, during the period of illumination, plants are constantly releasing oxygen through the process of photosynthesis, however, the phenomena of pearling may or may not occur. Usually, when plants release oxygen, it is dissolved in the water column. However, there is a certain moment when

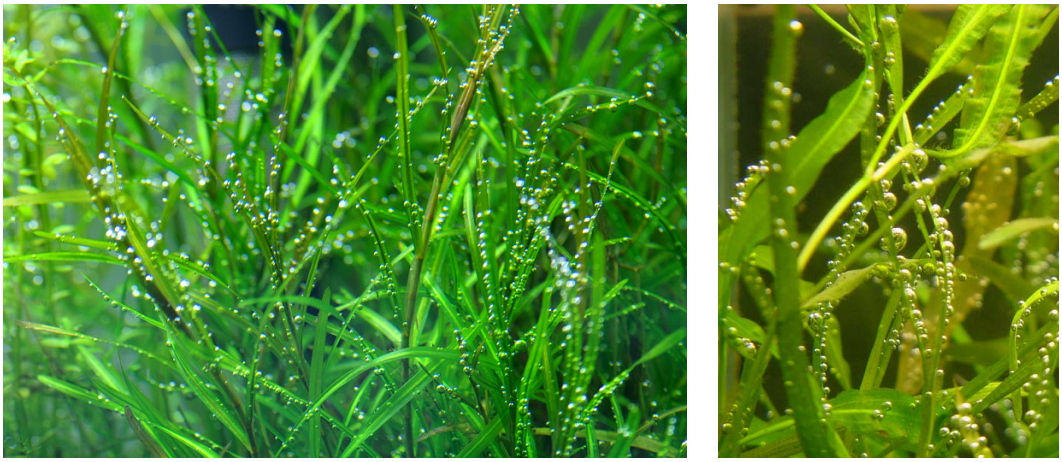

Figure 2.9: Pearling phenomena, bubbles released by marine plants (Aquariums, 2007).

the water column is saturated due to the high concentration of oxygen. When this occurs, the oxygen is released by the plants' leaves in the form of bubbles to the surface of the water column, as shown in the Figure 2.8.

For this reason, the greater the number of marine plants in an ecosystem, the greater the probability that they will saturate the water column more quickly and therefore there will be greater release of oxygen bubbles. During the night period, marine plants also consume the oxygen present in the water column which causes the oxygen level to decrease at night and only after a few hours of sun exposure is the water column saturated again.

This phenomena is very important for the study of underwater acoustics because the bubbles in water attenuate the acoustic signal and change the effective velocity of sound in the water. Throughout this master's thesis, it is possible to verify these phenomena caused by the oxygen bubbles.

3

Principles of Acoustic Quantification of Gas Bubbles by Travel Time Measurement

In the ocean, gas bubbles are formed from different natural and anthropogenic processes, such as wave breaking beneath the sea surface, ship's wake, underwater vents, gas hydrates on the ocean bottom, decomposition of organic material, photosynthesis of marine plants, etc (Medwin & Clay, 1998). The impact of bubbles in the acoustic signal along with methods to estimate their characteristics (sizes distributions, densities) have been reported by several authors as Medwin & Clay (1998); Vagle & Farmer

(1998); Terrill & Melville (2000). In general, these methods rely on the scattering and absorption properties of bubbles for signals in the frequency band of bubbles resonance, and the decrease of effective sound speed of the bubbly water for low-frequency signals. Simplified relations for the characterization of underwater air bubbles in response to acoustic signals may be considered when the pressure amplitudes are small, the gas void fraction (fraction of air bubbles to the volume of water) is small and the product of signal wavenumber (k) and bubble radius (b) is also small ($kb < 1$).

Detailed analysis of underwater sound propagation in bubbly environments can be found in Medwin & Clay (1998) and Brekhovskikh & Lysanov (2003). The volume of air bubbles formed during photosynthesis is expected small , therefore simplified relations for the analysis of sound propagation in bubbly environments can be considered.

The air bubble acts as a scatterer, which is characterized by the so called scattering cross-section (the ratio between the acoustic power scattered by and object to the incident wave intensity). The scattering cross-section of a bubble as the maximum at bubble resonance frequency f_0 is given approximately by Brekhovskikh & Lysanov (2003).

$$f_0 = \frac{3.27}{b}\sqrt{1 + 0.1D} \tag{3.1}$$

where z is the depth. As an example, the resonance frequency of a bubble of radius $100\mu\, m$ at $1m$ depth is $\approx 34\, kHz$. When a bubble is insonified at its resonance frequency the scattering cross-section (σ_s) reaches the maximum given by

$$\sigma_s = \frac{\lambda_0^2}{\pi} = \frac{c^2}{f_0^2 \pi} \tag{3.2}$$

where c is sound speed of the water. At frequencies well below ($f \ll f_0$) and above ($f \gg f_0$) of the resonance frequency, the scattering cross-section is given by

$$f \ll f_0 \qquad \Longrightarrow \qquad \sigma_s = 4\pi a^2 \left(\frac{f}{f_o}\right)^2$$

and

$$f \gg f_0 \qquad \Longrightarrow \qquad \sigma_s = 4\pi a^2$$

respectively. Thus, the intensity of the field scattered by the bubble is significantly lower as the frequency of the acoustic signal deviates from the bubble resonance frequency. Moreover, for frequencies well above the resonance frequency the intensity of the scattered field does not depend on the frequency. More accurate relations, which account for shear viscosity, thermal conductivity and other loss factors can be found in Medwin & Clay (1998); Brekhovskikh & Lysanov (2003), but their influence is not so important for the present qualitative analysis. The major differences are a down shift of the resonance frequency and a decrease of the scattering cross-section particularly close to the resonance frequency.

In the ocean, where bubbles with various radius coexist, the intensity of the overall scattered field results from an integral value encompassing the scattering cross-sections and density of bubbles (number of bubbles per unit volume) of different sizes (see Medwin & Clay (1998); Brekhovskikh & Lysanov (2003)), that can be measured by a backscatter device (Vagle & Farmer, 1998).

On the other hand, an acoustic signal propagating through a bubbly sea water suffers attenuation due to scattering and absorption. This excess attenuation is characterized by the so called extinction cross-section (similar to the scattering cross-section). The intensity of the acoustic signal decreases exponentially with propagating distance, where the attenuation coefficient is an integral value encompassing the extinction cross-sections and density of bubbles of different sizes. Various methods have been proposed for estimating bubble populations and size distributions using short range transmission of acoustic signals (Terrill & Melville, 2000).

Simpler methods have been developed taking into account that a small fraction of air bubbles to the volume of water (gas void fraction) has a very significant effect on the compressibility of the mixture, given rise to a decrease of the sound speed (com-

pared with bubble free water). The sound speed of the bubbly water is dispersive (frequency dependent), but for frequencies well below the bubbles resonance frequency, sound speed is simply a function of the void fraction (Terrill & Melville, 2000). Then, the medium sound speed c_e (effective sound speed) is given by the Wood's equation (Wilson & Dunton, 2009)

$$\frac{1}{c_e^2} = \frac{(1-\chi)^2}{c_w^2} + \frac{\chi^2}{c_g^2} + \chi\,(1-\chi)\,\frac{(\rho_g c_g)^2 + (\rho_w c_w)^2}{\rho_w \rho_g (c_w c_g)^2}, \tag{3.3}$$

where χ is the void fraction, c_w,c_g are the bubbles free water sound speed and gas sound speed, and ρ_w, ρ_g are the respective densities.

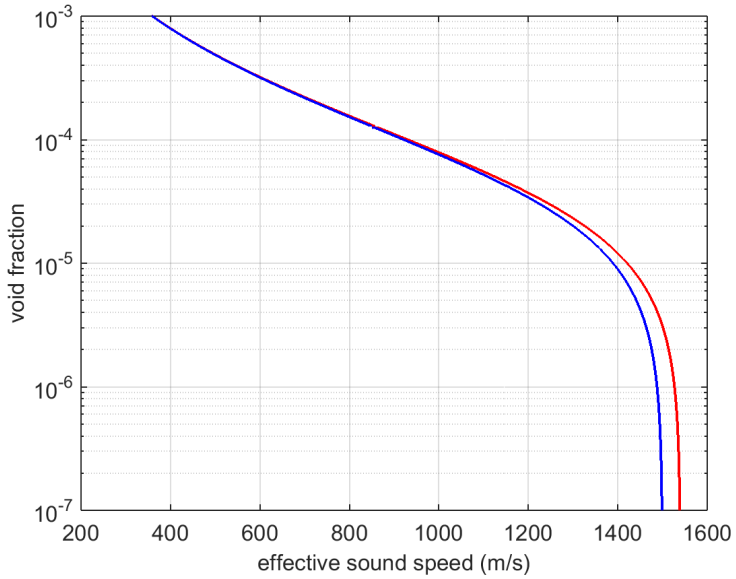

Figure 3.1: Air bubbles void fraction as a function of effective sound speed for two different sound speed of bubbles free sea water: 1500 m/s (blue) and 1540 m/s (red).

This property has been used by several authors to determinate the gas void fraction by estimating the effective sound speed from travel time measurements using setups where the source and the receiver are close located (Vagle & Farmer, 1998; Terrill & Melville, 2000; Wilson & Dunton, 2009; Lamarre & Melville, 1995). Figure 3.1 shows the air void fraction as a function of the effective sound speed for different sound speeds (1500 and 1540 m/s) of bubble free water. It can be noticed that, for gas void

fractions of order 10^{-4}, or higher, small differences in the gas free sound speeds can be neglected.

It should be remarked that, in general, commercially available devices commonly known as SVP (sound velocity profiler) can not be used to estimate the effective sound speed of bubbly water because it operates at very high frequencies, well above of the resonance frequency of the bubbles of interest. Under these conditions the signal suffers significant attenuation due to bubbles, but the sound speed tends to the bubbles free water sound speed.

3.1 Travel time measurements using low frequency pulses

Figure 3.2 depicts the setup used for sound speed estimation from travel time measurements. It is assumed that sound speed of the water c_e is constant between the sound source and the receiver, which are separated by a distance r, and both at a distance h from the bottom. Under these conditions, the path length of the direct echo (l_d) is equal to r.

In addition to the direct echo, the bottom and the surface reflected echoes between the source and the receiver should be also considered. The path length of the reflected echoes, l_b and l_s, are given by

$$l_b = \sqrt{r^2 + (2h)^2}, \tag{3.4}$$

$$l_s = \sqrt{r^2 + [2(D-h)]^2}, \tag{3.5}$$

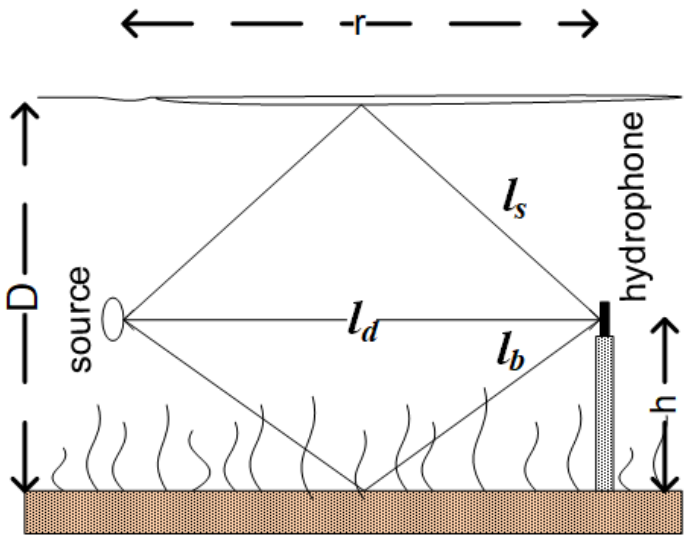

Figure 3.2: Measurement scheme for sound speed estimation based on travel time measurements.

where D is the water depth. The travel time of the various echoes are then given by

$$\tau_d = \frac{l_d}{c_e}, \tag{3.6}$$

$$\tau_b = \frac{l_b}{c_e}, \tag{3.7}$$

$$\tau_s = \frac{l_s}{c_e}. \tag{3.8}$$

The probe signals commonly used in such measurements are gated sinusoids (CW pulses), i.e a few cycles (N) of a tone at frequency f. The total duration of the probe signal is:

$$T_w = \frac{N}{f} \tag{3.9}$$

Thus to avoid overlap between the direct and reflected arrivals the following condition must be verified (min is the operator minimum value in a set):

$$\tau_d + T_w \leq \min\{\tau_b, \tau_s\}. \tag{3.10}$$

For a given geometry and signal duration, if (3.10) applies for the largest sound speed (i.e bubbles free water, c_w), then it applies for other sound speeds (i.e bubbly water). Therefore, bubbles free water sound speed ($\approx 1500\,m/s$) is the limiting sound speed to be considered in the measurement setup. From a theoretical standpoint, the source-hydrophone distance (r) and the pulse duration (T_w) should be the shortest as possible to fulfill (3.10) in very shallow water environments, particularly in low tide when the path of at least one of reflected echoes is the shortest. To determine the bubbles concentration based on the effective sound speed of the water, the frequency of the probe signal should be well below of the bubbles resonance frequency, i.e. low frequency/long cycle signals must be used. The size and thus the resonance frequency of bubbles formed during photosynthesis are not known, but it is expected that pulses at frequencies below 20 kHz are well suited for effective water sound speed estimation. Moreover, a minimum pulse length is required for the probe signal to reach the steady-state, when the measurement might be performed. The pulse length is usually measured in a number of cycles and depends on the source characteristics. Minimal pulse length between 2 to 6 cycles are usually required to the source reach the steady state.

To perform the travel time measurement, the receiver should be placed in far-field region of the source, where the pressure decreases smoothly ($\sim 1/r$) with increasing range. The far-field condition constrains the minimal distance between the source and the receiver, which depends on several aspects, like the dimensions and shape of the source and the frequency of the signal. As a rule of thumb the far field of a source exists at a distance greater than a^2/λ, where a is the largest active dimension of the source and λ is the signal wavelength ($\lambda = c_e/f$) (Au & Hastings, 2008). Therefore, the minimal far-field distance increases as the frequency decrease. The fulfillment of the above mentioned constraints by the measurement system will be assessed during tanks tests, which will serve as calibration tests for the system described in the following chapter.

4

Measurement system

The system will be based on precise measurements of travel time, therefore the sound source and the receiver will be accurately synchronized. Such a system will provide accurate results and will serve as a baseline for the calibration of bubbles quantification methods at the pond level. Herein, the implementation of the system is discussed , and preliminary tank tests are presented.

Figure 4.1 presents a block diagram of the measurement system, showing the various components and their links. The whole acquisition process (signal generation, data recording and storage) is controlled by a Red Pitaya board. Signal generator and an oscilloscope to display simultaneously the waveforms at various points of the transmitting and receiving chain were used for testing and control the system equipment.

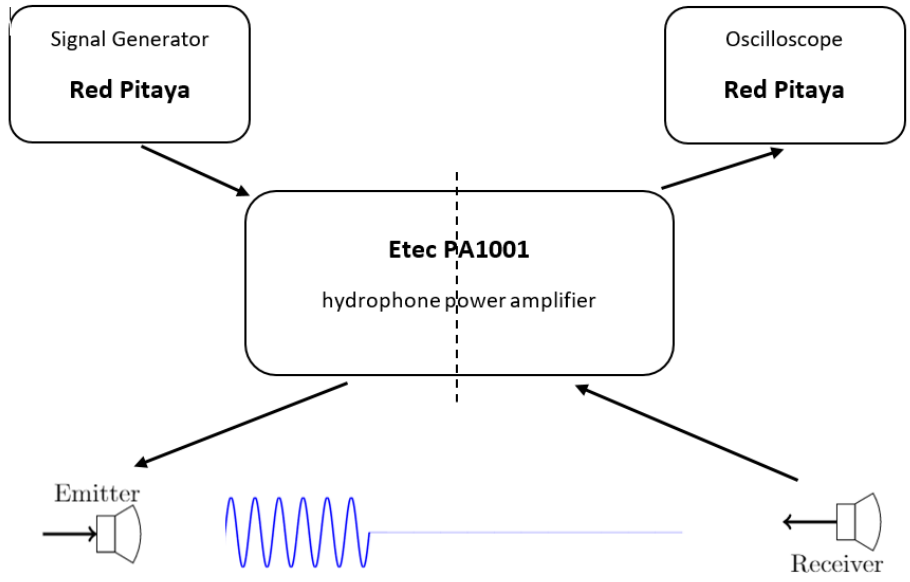

Figure 4.1: Block diagram of the measurement system.

The transducers used to transmit and receive the acoustic signal were the RESON TC4033 and the ITC-2044. The amplifiers used in the system are the PA1001 power amplifier and CA1702 charge amplifier from ETEC.

4.1 System equipment

4.1.1 Transducers

As stated above, the transducers used in the experiments were the RESON TC4033 and the ITC-2044. Both can be used as transmitter or receiver, but in the present tests, the former was used in both operating modes, whereas the later only as transmitter.

The RESON TC4033 is a small spherical (2.5 cm diameter), as shown in Figure 4.2, broadband (1–140 kHz), omnidirectional underwater acoustic transducer. The resonance frequency is around 100 kHz and the linear frequency range is 1-80 kHz, where the receiving sensitivity (see Figure 4.5) is about $-203\,dB\ re\ 1V/\mu Pa$. (the RESON TC4033 transducers used in this project were individually calibrated with long cables of 20 meters). The transmit voltage response (TVR) of this transducer is shown in Fig-

ure 4.3. As expected, the maximum TVR (145 $dB\,re\,1\mu Pa\,@\,1m$) is at the resonance frequency. The TVR at lower frequencies is significantly smaller (95 $dB\,re\,1\mu Pa\,@\,1m\,@5\,kHz$) due to the small transducer dimensions. The TVR increases at a ratio of 20 dB per decade in the linear frequency range of the transducer. The acoustic power at 1 m from the source is often given by the source level (SL) as

$$SL = TVR + 20\log(V), \quad (dB\,re\,1\mu Pa\,@\,1m) \tag{4.1}$$

where V is the input voltage of the transducer and log is the decimal logarithm. Therefore, considering the characteristics of the RESON TC4033 and the PA1001 power amplifier, the maximum SL achievable at 5 and 15 kHz are 125 and 145 $dB\,re\,1\mu Pa\,@\,1m$, respectively.

Figure 4.2: Tranducers used in the system. The RESON TC4033 on the left and ITC-2044 on the right.

As the transmitter and the receiver will be placed at short distance ($\sim 1\,m$ see below), the spreading loss will be small, however, the bubbles might attenuate significantly the signal. An excess attenuation of about 6 dB due to bubbles released during photosynthesis was measured in CW pulses at 15 kHz during a previous experiment in the pond where the measurement system will be installed (Felisberto et al., 2017b). Moreover, the noise power in the pond is large (Felisberto et al., 2017b), so a large SL is required to achieve a large SNR (with low SNR the uncertainty of the sound speed measurements increase (Lamarre & Melville, 1995)). In order to increase the SL in the band of interest the transducer ITC-2044 was also considered. The ITC-2044 transducer is a cylindrical transducer (9.5 cm diameter, 4.5 cm height), as shown in Figure 4.2, with a toroidal beam pattern. The usable frequency band is 6-16 kHz, what fits the need of this project. The TVR is approximately flat between the 8–14 kHz ($135 dB\,re\,1\mu Pa\,@\,1m$), as shown in Figure 4.4. Therefore, in the band of the interest this transducer provides more 15 dB at least. However, it should be remarked that the ITC-2044 was not calibrated (only the catalog curves are available).

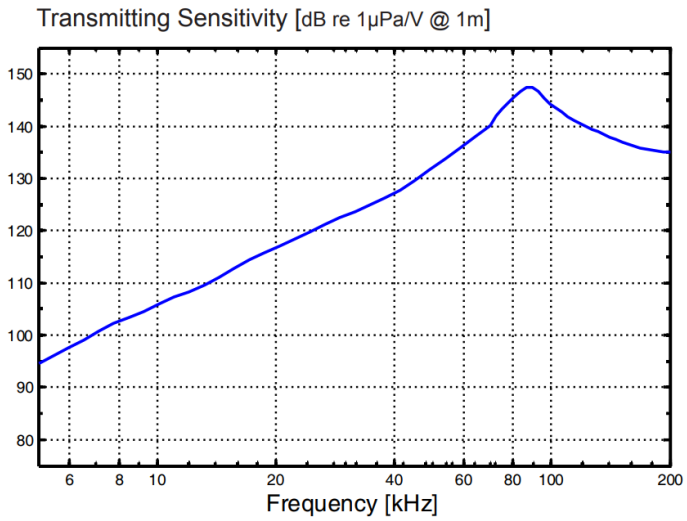

Figure 4.3: Transmit Voltage Response of transducer RESON TC4033 (from devices catalog).

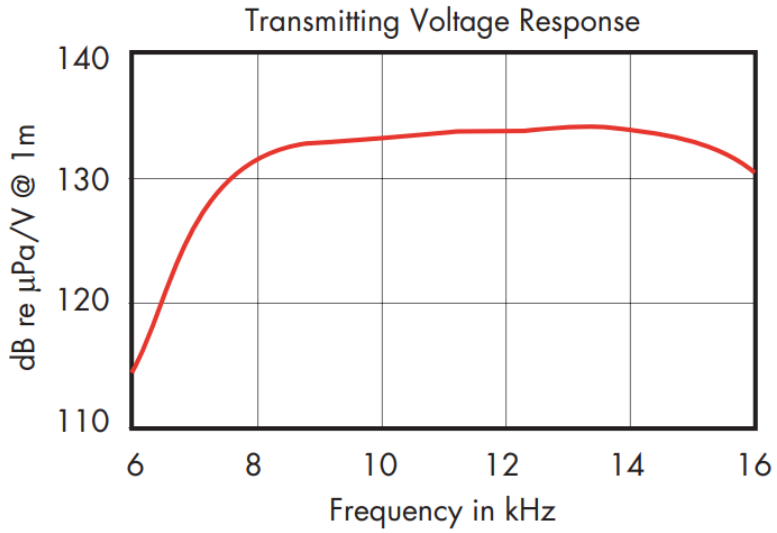

Figure 4.4: Transmit Voltage Response of transducer ITC-2044 (from devices catalog).

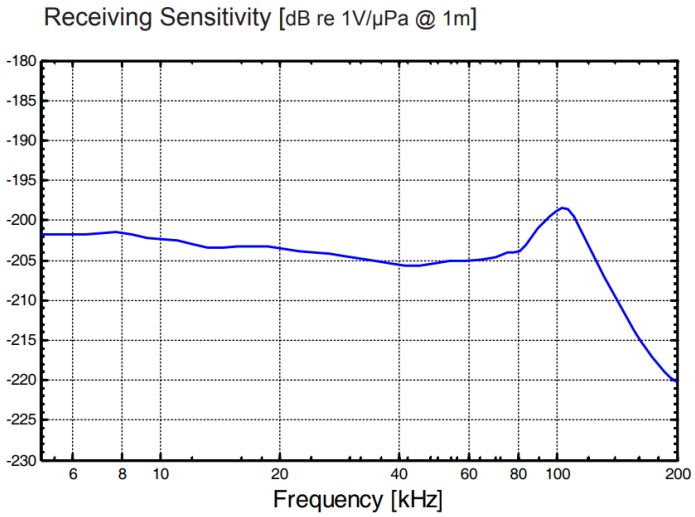

Figure 4.5: Receiving sensitivity of RESON TC4033 (from device catalog).

As discussed in Section 3.1, in very shallow water environments the minimal pulse length (number of cycles) might be a critical parameter to avoid interference of reflected echoes on the direct echo, particularly when low frequency CW pulses are used. It was found experimentally that at least 4 cycles long CW pulses should be used for the signal to reach the steady state (particularly for the ITC-2044 this is the very low limit). However, the transients at signal turn-on and turn-off are different

for both transducers, as can be seen in Figure 4.6, where the left panel is from the REASON TC4033 transducer and the right panel is from the ITC-2044 transducer.

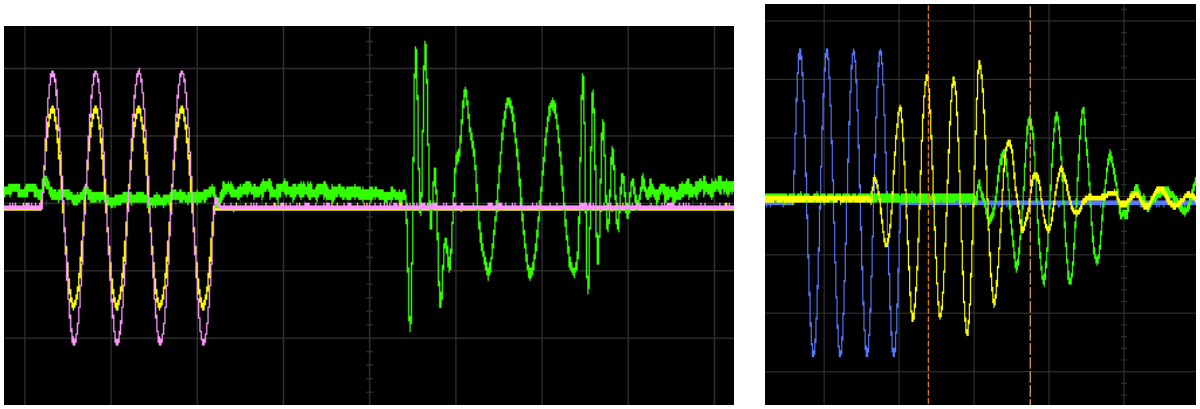

Figure 4.6: Waveforms generated by the transducers when driven by 4 cycle long CW pulse at 10 kHz: RESON TC4033 (on the left) and ITC-2044 (on the right). In both cases the initial superimposed waveforms are at the input and output of the power amplifier. The green waveforms (and yellow on the left) were acquired by RESON TC4033 receiver in the far-field of the transmitter, but at a close distance ($\sim$ 70 cm). The delays are related to the travel time (the time scales are different among figures, and the amplitude scales are different among waveforms)

In both cases, 4 cycles long CW pulses at 10 kHz were generated by a signal generator and amplified by the PA1001 amplifier. The various waveforms superimposed at the beginning of both panels in Figure 4.6 are at the output of the signal generator and at the output of the amplifier, showing undistorted waveforms at this point. It should be noted that the time scales are different among panels, and amplitude scales are different among waveforms. The waveforms were gathered by RESON TC4033 transducers, displayed in green, in both panels and also in yellow in the right panel, where two receivers were used. The receivers were in the far-field of transmitters, nevertheless at close distances ($\sim$ 70cm). The different characteristic oscillations at the turn-on

(raise) and turn-off (tail) transients of the CW pulse transmitted by the transducers are related to the respective resonance frequencies. These transients should be accounted by the travel time estimation methods, otherwise, the results should be affected by significant errors. Using windowed CW pulses, the transients can be reduced, at an expense of longer signals (see Au & Hastings (2008) for details).

4.1.2 Power Amplifier

The hydrophone and underwater loudspeaker power amplifier that was used in the system is the Etec PA1001PC Power amplifier and Two-Channel Charge amplifier also from Etec.

Etec PA1001PC Power amplifier

The PA1001 amplifier from ETEC, Denmark was used for driving sound transmitter and for conditioning and amplifying the signal from the receiver. The amplifier has a highly sensitive input impedance hydrophone preamplifier for passive or active piezoceramic transducers and is capable of driving 90 V peak-to-peak (32 V rms) of signal up to 300 kHz. It also contains a high input impedance hydrophone (receiver) amplifier with the possibility of different gain.

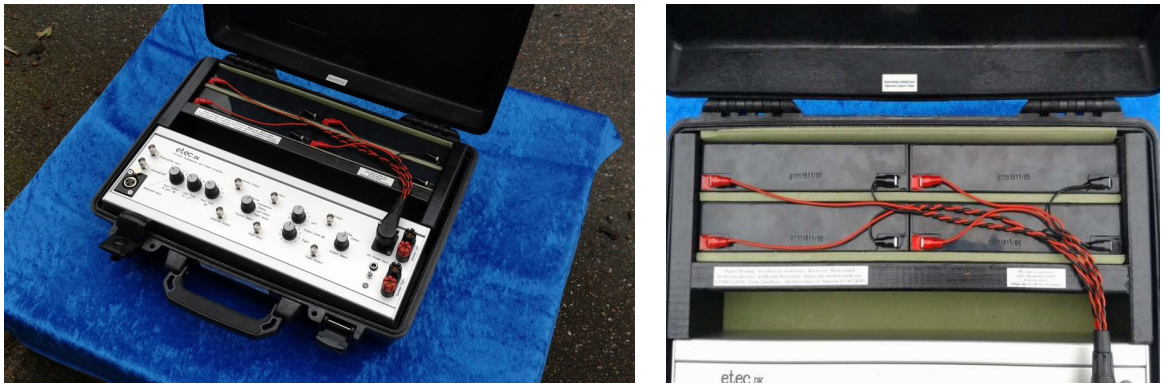

Figure 4.7: Etec PA1001PC Power amplifier in watertight suitcase (on the left) and four batteries pack (on the right).

For the field experiments foreseen in the SEAOX project, long cables (20 m) are required to connect the transducers to the amplifier. Because, the transducers have to operate in transmitting mode, built-in pre-amps were not available. Therefore, the PA1001 was modified to include an input circuit to compensate for the signal loss due to the long cables.

Basically, the PA1001 is a stand-alone unit with a power amplifier and a hydrophone receiver amplifier complete with batteries and charger supplied all together in a watertight suitcase, as shown in Figure 4.7 on the left.

This power amplifier is supplied in a watertight suitcase with 4pcs. 12V 3.4Ah batteries, as shown in Figure 4.7 on the right. Operating time is approximately 12 hours on a set of fully charged batteries and the approximate maximum charge time is about 24 hours. It is also possible to operate with the amplifier connected to the charger which is very useful for the study of bubbles production during various diurnal periods.

Figure 4.8: Hydrophone charge amplifier and preamplifier inputs module.

This module, shown in the Figure 4.8, includes an input circuit to compensate for the signal loss due to the long cable, including one charge amplifier to attenuates the

unexpected noise. It also includes the preamplifier to amplify the input signal to be noise tolerant and for further processing. Finally, this module is also equipped with a high-pass filter to filter the low frequencies.

The purpose of the ***charge amplifier input*** is to connect any passive hydrophones with long cables and BNC connector. The charge amplifier is in fact much more immune to the hum and noise pickup compared to normal voltage amplifiers.

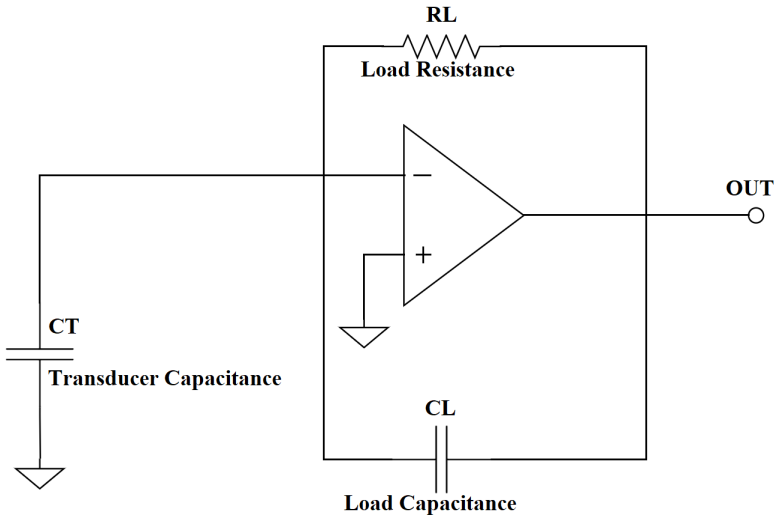

Figure 4.9: Charge amplifier schematic

The philosophy of the charge amplifier is that the signal from the transducer enters the summing point of the amplifier which in general is at zero potential because the positive input of the amplifier is grounded. Therefore we have zero voltage on the transducer cable and since there is no voltage we cannot get false signals induced from outcoming electrical fields.

Input gain is equal to the transducer capacitance divided by load capacitance (in case of the *charge amplifier input* the load capacitance is equal to 1nF):

$$Input\ \ Gain(dB) = 20 * log(\frac{transducer\ \ capacitance}{load\ \ capacitance}) \tag{4.2}$$

For example, with the equipment used throughout this master thesis, it is possible to calculate the input gain of the amplifier. As stated above, in Section 4.1.1, the transducers RESON TC4033 used as the receivers have a cable of 20 meters in length. The manufacturer of the hydrophone presents in the datasheet of the RESON TC4033 the value of 7.8 nF for the nominal capacitance of the hydrophone including 10 meters of cable. Moreover, adding extra cable increases the capacitance by between 100 pF and 150 pF per meter. Therefore, in this case, is necessary to increase the capacitance considering only 10 meters of cable, since the other 10 meters are already included in the nominal capacitance of the transducer. That is, the capacitance has to be increased between 1 nF and 1.5 nF.

Finally, the input gain of the amplifier is easily deduced by the formula 4.2. This value is calculated below, for both cases (1 nF and 1.5 nF, respectively):

$$Input\ \ Gain(dB) = 20 * log(\frac{7.8\ \ nF\ \ +\ \ 1\ \ nF}{1\ \ nF}) \approx 18.9\ \ dB \tag{4.3}$$

$$Input\ \ Gain(dB) = 20 * log(\frac{7.8\ \ nF\ \ +\ \ 1.5\ \ nF}{1\ \ nF}) \approx 19.4\ \ dB \tag{4.4}$$

With this, it is possible to conclude that the input gain of the amplifier is approximately 19 dB, under these conditions. This value has already been experimentally verified, in an experiment performed in the framework of another research project in which this equipment was used.

The ***High Pass*** filter is controlled by the load resistance (RL) and load capacitance (CL), shown in Figure 4.9, and is given by the following equation:

$$High\ \ freq.\ \ Limit\,(Hz/-3dB) = \frac{1}{2.\pi.RL.CL} \tag{4.5}$$

Filter slopes are 6 dB/octave and values possibles to frequency limit are 10 Hz to 3 kHz. The big advantage of this for the measurement system is to eliminate the low frequencies, thus increasing the dynamic range for the frequencies of interest.

The ***Input Gain*** is a linear input amplifier to offering extra gain 10 Hz to 1 MHz.

Figure 4.10: Power amplifier

With this power amplifier, it is possible to obtain output power level about of $\pm$ 48V peak if the ***Output Select*** is in the **Bridge** position. In **Bridge** configuration the load must be connected to the left and right red terminals thus forming a balanced floating output. The signal must be connect to ***Left Input*** or ***Right Input*** depending on the selection made on ***Source Select***. The ***Output Level (dB)*** left or right is to control the level for the output power amplifiers. Near the black and red terminals, there is a switch button to turn ON and OFF the whole amplifier system and a connector to connect the batteries or the charger. In this project, it was used only ***Left mono*** to transmit signal by the hydrophone.

Data	Values
High Pass (Hz)	10 / 30 / 100 / 300 / 1k / 3k
Input Gain (dB)	0 / +6 / +12 / +18 / +24 / +30
Output Level (dB)	0 / -3 / -6 / -9 / -12 / -15 / -18 / -22 / -26 / -30 / -34

Table 4.1: Technical data about Etec PA1001PC Power Amplifier

Two Channel Charge Amplifier

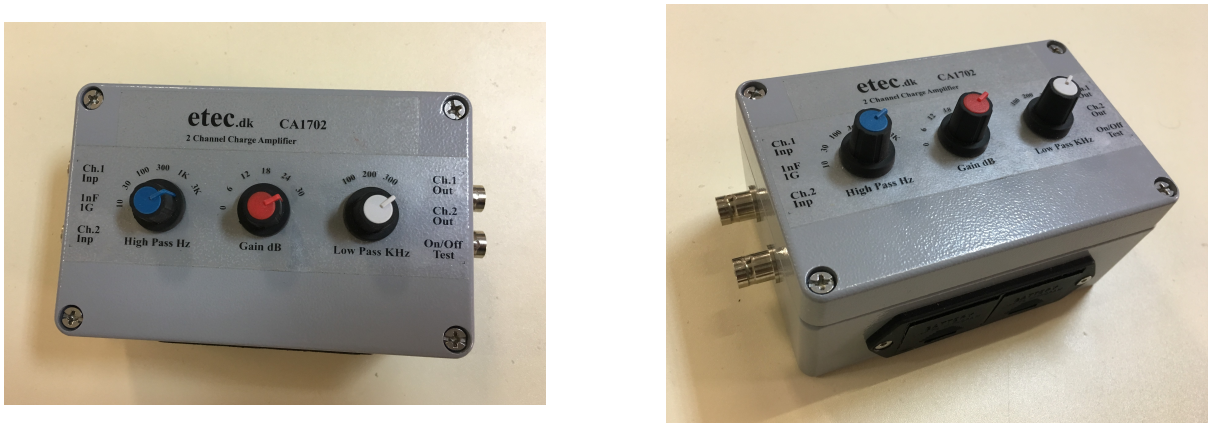

Figure 4.11: Two channel charge amplifier, Etec CA1702

To use two hydrophones as receivers, as shown in Figure 4.17 on the bottom (setup TRR), was used two-channel charge amplifier from Etec. The operation of this amplifier is similar with the charge amplifier previously explained in this section, but the only difference is that this amplifier has two channels, so its possible to connect two receiver hydrophones simultaneously. This equipment is powered by an internal battery, basically two 2 pcs. build-in 9 V PP3 batteries. Operating time is approximately 48 hours on a set of fully charged batteries (this operating time was tested in an experimental test, shown in Section 5.2.2).

Data	Values
High Pass (Hz)	10 / 30 / 100 / 300 / 1k / 3k
Gain (dB)	0 / +6 / +12 / +18 / +24 / +30
Low Pass (kHz)	100 / 200 / 300

Table 4.2: Technical data about two-channel charge amplifier

4.1.3 Acquisition board

The measurement system will be controlled by a Red Pitaya (RP) board, which hardware and software were initially conceived as a tool to replace expensive laboratory measurement instruments such as the oscilloscope, spectrum analyzer and signal generator. The core of the RP is a dual ARM Cortex A9 and a FPGA. The board includes an ADC LTC2145CUP-14 and a DAC DAC1401D125HL DAC, both with two channels, 14 bits of resolution and a sampling frequency up to 125 MHz. The maximum output voltage is 2 V peak to peak. The system is powered by a micro USB cable with 5 V supply, and can be connected to a battery or directly to the main voltage. The system and FPGA image is flashed into a micro SD card. For the internet connection, there is a 100 Mbit ethernet port, used in this project to connect to a laptop for data monitoring and storage. There are two options for connecting to the RP, connect the computer to the same network as the RP and access the address of the board or use the WI-FI connection from the RP and connect the computer directly to the network of the RP board. This option allows controlling the measurement system remotely through a wifi connection, for this, only need a WI-FI dongle connected to the USB port of the acquisition board. The procedure for connecting the computer to the Red Pitaya board via the WI-FI connection is explained step-by-step in Appendix A.

After the connection is made, the RP was programmed through a MatLab script (using SCPI commands and TCP/IP communication) to generate and acquire signals.

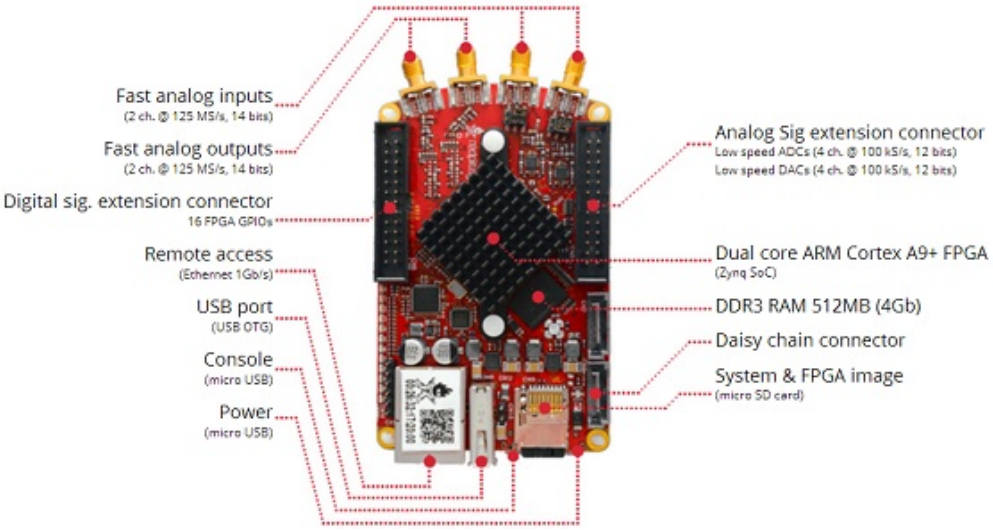

Figure 4.12: Schematic of the Red Pitaya (retrieved from the Red Pitaya manual).

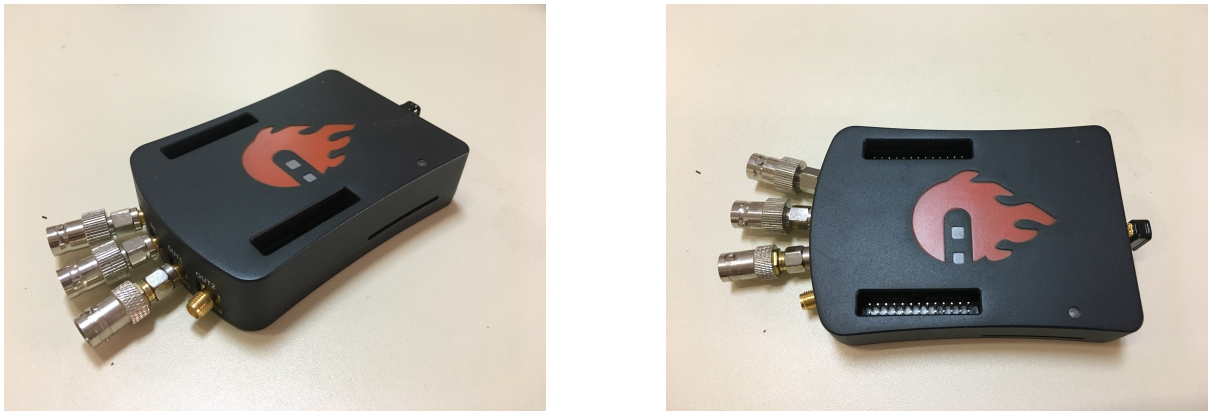

Figure 4.13: Red Pitaya acquisition board with aluminium case to protect board very well against mechanical, environmental and EMI effects.

4.2 System Installation and Operation

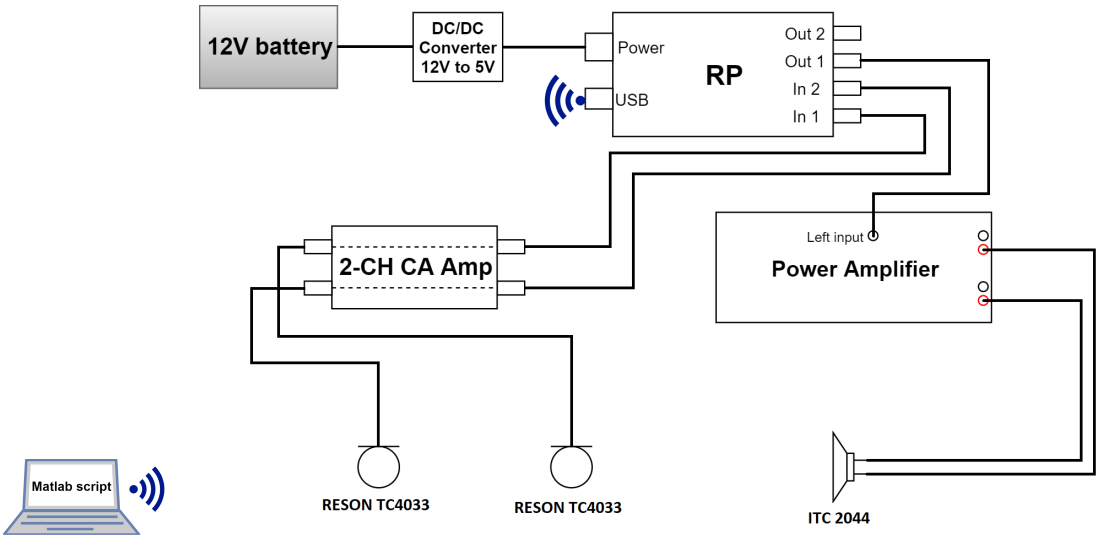

Figure 4.14: System diagram

The installation of the system according to the setup TRR (see in Section 4.3 and Figure 4.17) is depicted in the diagram in figure 4.14. The Red Pitaya (RP) acquisition board is supplied through the 12V battery connected to DC/DC converter to change the voltage from 12V to 5V. The connection of RP to the PC is made through the wireless connection, as shown in the user manual in appendix A. Wireless connection is supported on the RP via a USB adapter, in this case, the USB adapter used is the Edimax-EW7811UN. The PC controls the entire generation and acquisition system though the MatLab script. The signal is generated and sent through port ***Out1*** of the RP to the power amplifier that transmits the amplified signal to the transmitter hydrophone, the ITC-2044. The signal received by the RESON TC4033 hydrophones is amplified by the two-channel charge amplifier and then connected to the ***In1*** and ***In2*** ports of the RP to be acquired. If instead of setup TRR is used setup TR (see in Section 4.3 and Figure 4.17), the only change is to connect only one of the channels of the two-channel charge amplifier.

MatLab script use SCPI commands and TCP/IP communication. The script generates the signal that the user sets, normally a burst with 2 or 4 cycles at the defined

frequency. The acquired signals are transmitted simultaneously and the trigger is executed on the sent signal. In this way, there is synchronism between the signals received and generated being easily measured the propagation times of the signals through special points of the signals, for example, the signal peaks (as shown in Section 4.2.1).

This script has been optimized to be able to generate and acquire signals of one single frequency or send sequences of signals of a range of frequencies. For this, it is necessary to set start and end frequency, the number of times that each signal of each frequency was transmitted and the number of repetitions of that sequences.

The Red Pitaya board has the buffer with 16384 samples. Time length of the acquired signal depends on the time scale of a buffer that can be set with a decimation factor. Decimations and time scales of a buffer are given in the table below.

Decimation	**Sampling rate**	**Time scale/length of a buffer**
1	125 MS/s	131.072 μs
8	15.6 MS/s	1.049 ms
64	1.9 MS/s	8.389 ms
1024	122.0 kS/s	134.218 ms
8192	15.2 kS/s	1.074 s
65536	7.6 kS/s	8.590 s

Table 4.3: Decimation, Sampling rate and time length of the buffer of Red Pitaya

Usually, the sampling rate used is 1.9 MS/s (Mega-Samples per second), so a decimation of 64 is made. The user can define several parameters in the case that signals of a single frequency are sent, as shown in Table 4.4. The parameters that the user can set in the case of the sequence of signals are shown in the Table 4.5.

The SCPI commands required to be programmed through MatLab software can be easily consulted at documentation of Red Pitaya (StemLab, 2016).

Parameter	Description	Range of values
Number of acquisitions	Number of acquisitions to be made and saved during transmission	0 ... INF
Delay between acquisitions	Time in seconds between acquisitions	0 ... INF*
Type of signal	Different waveforms can be transmitted, including one external signal	Sine, Square, Triangle, PWM, Arbitrary
Frequency of signal	Number of occurrences of a repeating event per unit time (kHz)	0 ... 50 MHz
Amplitude	Amplitude of the signal (V)	0 ... 1
Burst mode	To turn ON or OFF the burst mode of the Red Pitaya	Y or N
Number of periods in one burst	Number of cycles of the one burst	1 ... INF

INF* - Large integer number but **not infinite**.

Table 4.4: Parameters that user can define in MatLab script to send signals of a single frequency.

The signals received on the two transducers are stored for each acquisition in a single TXT file. These signals have the size of the Red Pitaya buffer, ie 16384 samples. The TXT file name is recorded with the date, time and frequency of the corresponding transmitted signal, as shown in the following example:

20171201_145753_f10.txt $\Rightarrow$ 2017/12/01, 14:57:53 - 10 kHz signal

Parameter	Description	Range of values
Number of Repetitions	Number of repetitions per each frequency	0 ... INF*
Number of Acquisitions	Number of transmitted sequences	0 ... INF*
Delay between repetitions	Time in seconds between repetitions of each frequency	0 ... INF
Delay between sequences	Time in seconds between of each sequences	0 ... INF
Type of signal	Different waveforms can be transmitted, including one external signal	Sine, Square, Triangle, PWM, Arbitrary (external signal)
Start Frequency	Start frequency of the transmitted sequence signal (kHz)	0 ... 50 MHz
End Frequency	End frequency of the transmitted sequence signal (kHz)	0 ... 50 MHz
Amplitude	Amplitude of the signal (V)	0 ... 1
Burst mode	To turn ON or OFF the burst mode of the Red Pitaya	Y or N
Number of periods in one burst	Number of cycles of the one burst	1 ... INF

INF* - Large integer number but **not infinite**.

Table 4.5: Parameters that user can define in MatLab script to send sequences of signals of a range of frequencies.

4.2.1 Peak detection and Measurements

The signals acquired by the transducers that were recorded in the TXT file are then processed in order to calculate the propagation times of the signals and their amplitudes.

First, the received signals are filtered through a bandpass FIR (*finite impulse response*) filter of MatLab of 1 kHz bandwidth centered at CW frequency. The objective of this operation is to reduce the out of the band noise in the received signal.

After filtering the signals, is performed the detection of the peaks of both direct propagation signals (first arrival). The peaks of both received signals (first and second receiver) are detected using the ***findpeaks*** function of MatLab. After the peaks are found, only the first peak of both signals is considered, as shown in Figure 4.15. The peaks of first received signal are represented by red circles and the second received signal by blue circles. The first peaks of both signal are represented by the yellow box. From these first peaks, the values of the times at which the peak occurs and its amplitudes are stored. With these values, are easily determined the values of attenuation between the two receivers and the sound speed in water, once that the two receivers are at a known distance.

Taking the example of Figure 4.15, the values taken from the first peak of each signal through the peak detection explained above, are shown in the Table 4.6.

As in this case the distance between the receivers is known (approximately 31.5 cm), the values of the attenuation and the sound speed are easily deduced, through the formulas 4.6 and 4.7, respectively.

$$Att = -20 \times log \frac{amplitude_{\text{peak}_2} \ (V)}{amplitude_{\text{peak}_1} \ (V)} \ [dB] \tag{4.6}$$

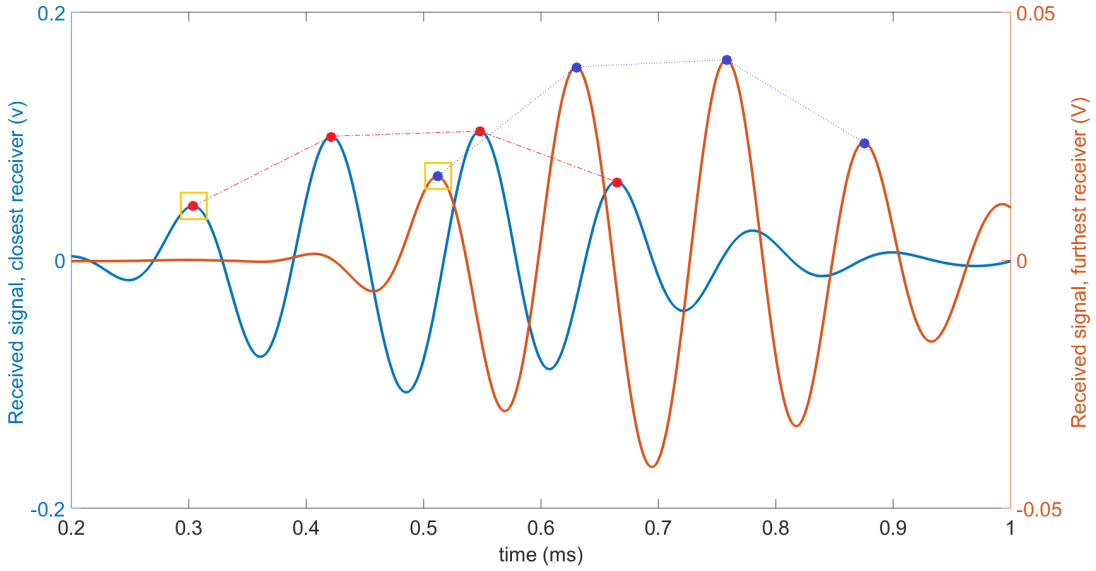

Figure 4.15: Example of peak detection in two signals acquired by RESON transducers. Peaks of the first receiver are represented by red circles and the second receiver by blue circles. The first peak of both signals is represented by the yellow box.

Point	Time (ms)	Amplitude of signal (V)
1st Peak of closest receiver	0.303104	0.042984
1st Peak of furthest receiver	0.512512	0.017511

Table 4.6: Measures of the values of Figure 4.15. Values of the closest receiver (on the top) and furthest receiver (on the bottom)

$$ssp = \frac{d_{\text{receivers}}\ (m)}{\Delta\ time\ (s)}\ [m/s] \tag{4.7}$$

where:

$amplitude_{\text{peak}_1}$	amplitude of the peak of the first receiver (closest receiver)
$amplitude_{\text{peak}_2}$	amplitude of the peak of the second receiver (furthest receiver)
$d_{\text{receivers}}$	distance between the two receivers (in meters)
$\Delta\ time$	time difference between the peaks of the two receivers (in seconds)

In Table 4.7 it is possible to verify all the calculations of the values of sound speed

Measure	
Sound Speed	$ssp = \frac{0.315}{(0.512512 - 0.303104) \times 10^3} \approx 1504.24 \ \ m/s$
Attenuation of signal	$Att = -20 \times log\frac{0.017511}{0.042984} \approx 7.8 \ \ dB$

Table 4.7: Example of measurements of sound speed and attenuation of the signal through the values found by peaks detection of the current example.

in the water and attenuation of the signal in case of the example of Figure 4.15. The obtained results allow to verify the correct operation of the whole system.

4.3 Setups

Several setups were considered in order to optimize the whole system. In this section, the system setups made initially are shown, which serve as a starting point for the development and improvement of the system. The final setup of the system is also shown, before setting the system to make measurements for a long period of time.

4.3.1 Primary setups

Initially, the system was calibrated by performing several experiments at the Aquaculture Research Station (IPMA-EPPO) of Portuguese Institute for the Sea and Atmosphere, Olhão, southern Portugal, in one tank with nothing inside, besides salt water and air bubbles.

The tank is a small ground tank with 5 m of length per 2.5 m of width and 1.8 m height. The tank was filled with saltwater up to 1.6 m water depth, as shows Figure 4.16. The tank is equipped with an aeration system with various simple bubble

releasers, which flow is controlled manually. However, the bubble size and flow are unknown.

This experience was the first where the data acquisition and generation system were implemented, essentially to do the first tests and to calibrate the whole setup.

Two setups were used: setup TR, similar to that shown in Figure 3.2 with two transducers; and setup TRR, an alternative setup with three transducers. It was used setup TRR to measure travel time related two equal hydrophones (RESON TC4033) and was used ITC-2044 as a transmitter, because this transducer has more power in low frequencies (below 20kHz). Figure 4.17 show the geometry of setup TR, on the top, and geometry of the setup TRR, on the bottom, where the transmitters are represented by the blue rings and the receivers by the red filled circles.

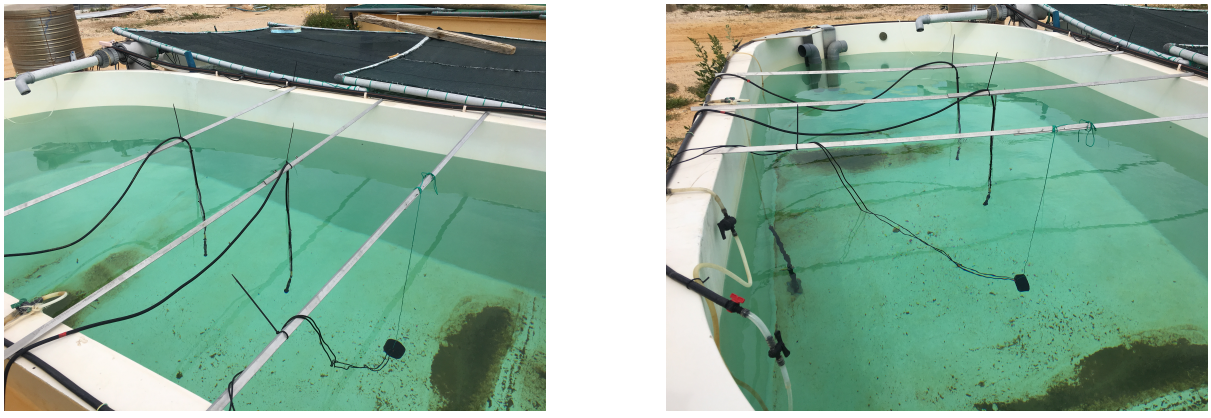

Figure 4.16: Transducers mounted in the tank (setup 2) in setup TTR (see Figure 4.17).

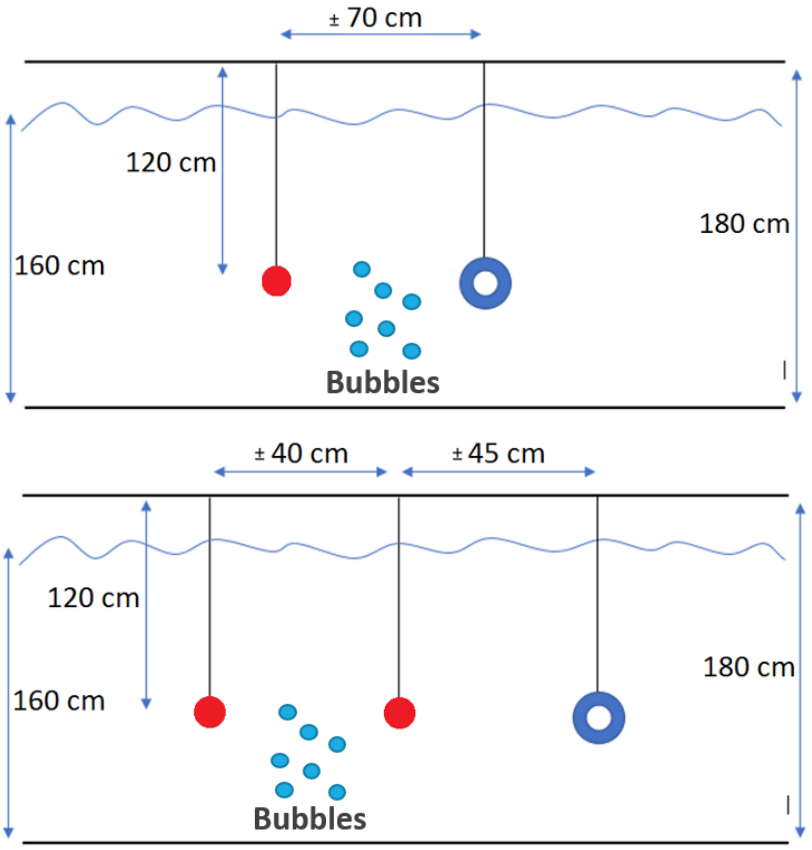

Figure 4.17: Geometry of setup TR (on the top) and setup TRR (on the bottom). The blue rings indicate the transmitter and the red filled circles indicate the receivers. The area where the bubbles are released is also shown in both setups.

Figure 4.16 shows the tank with the transducers mounted in setup TRR, with the ITC-2044 used as a transmitter and two RESON TC4033 as receivers. In both setups, the transducers were hung in the tank with the aid of stainless steel crossbars, vertically centered along the length, approximately at 2.5 m from the side walls, and 0.6 m from the bottom (1 m from the surface). In setup TR the transmitter-receiver distance is about 0.70 m and, in setup TRR the distance between receivers is about 0.42 m, and the distance from the transmitter to the closest receiver is about 0.45 m. Several distances between transducers were tested, but the results discussed below was obtained with the above geometry, which is believed to be closer to the field conditions.

Setup TR - Transmitter and One receiver

Figure 4.18 shows the 6 cycle long CW pulses at 10 kHz generated by the RP (red line) and the signals received at the RESON TC4033 transducer using setup TR (blue line). The upper panel represents the bubbles free case, and the bottom panel shows the case when bubbles were released between the transmitter and the receiver. The transmitter–receiver distance estimated from the travel time difference between the transmitted CW pulse and the first arrival (direct echo) in the bubbles free case was 72 cm (sound speed 1500 m/s).

When few bubbles were released between the transmitter and the receiver, the travel time only increased by 3 μs, and the attenuation by 12 dB. It can be seen a DC offset in the signals, which should be filtered for attenuation calculations. Please note the different amplitude scales used in the plots. Since, the ITC-2044 was not calibrated spreading loss was not calculated. In these tests the bubbles are released on a small confined area, therefore the reflected echoes (after the direct echo) are not analyzed herein. These later arrivals are due to reflections on the tank walls, bottom and surface.

Setup TRR - Transmitter and Two receivers

Figure 4.19 shows the signals received in two RESON TC4033 transducers in a setup TRR configuration. The signal transmitted by the ITC-2044 was a 4 cycle long CW pulse at 10 kHz. The signal acquired by the closest receiver to the transmitter is shown as a blue line, whereas the signal acquired by the receiver farthest away from the transmitter is shown as a red line. The upper panel represents the bubbles free case, and the bottom panel shows the case when bubbles were released between the receivers. During this test the bubbles flow was more intense than in the test using setup TR.

In both panels one can observe several echoes of the CW pulses. The first echo at the receivers represents the direct path. Therefore, the travel time of the direct echo between the receivers is obtained at corresponding points of the first echo in blue and red

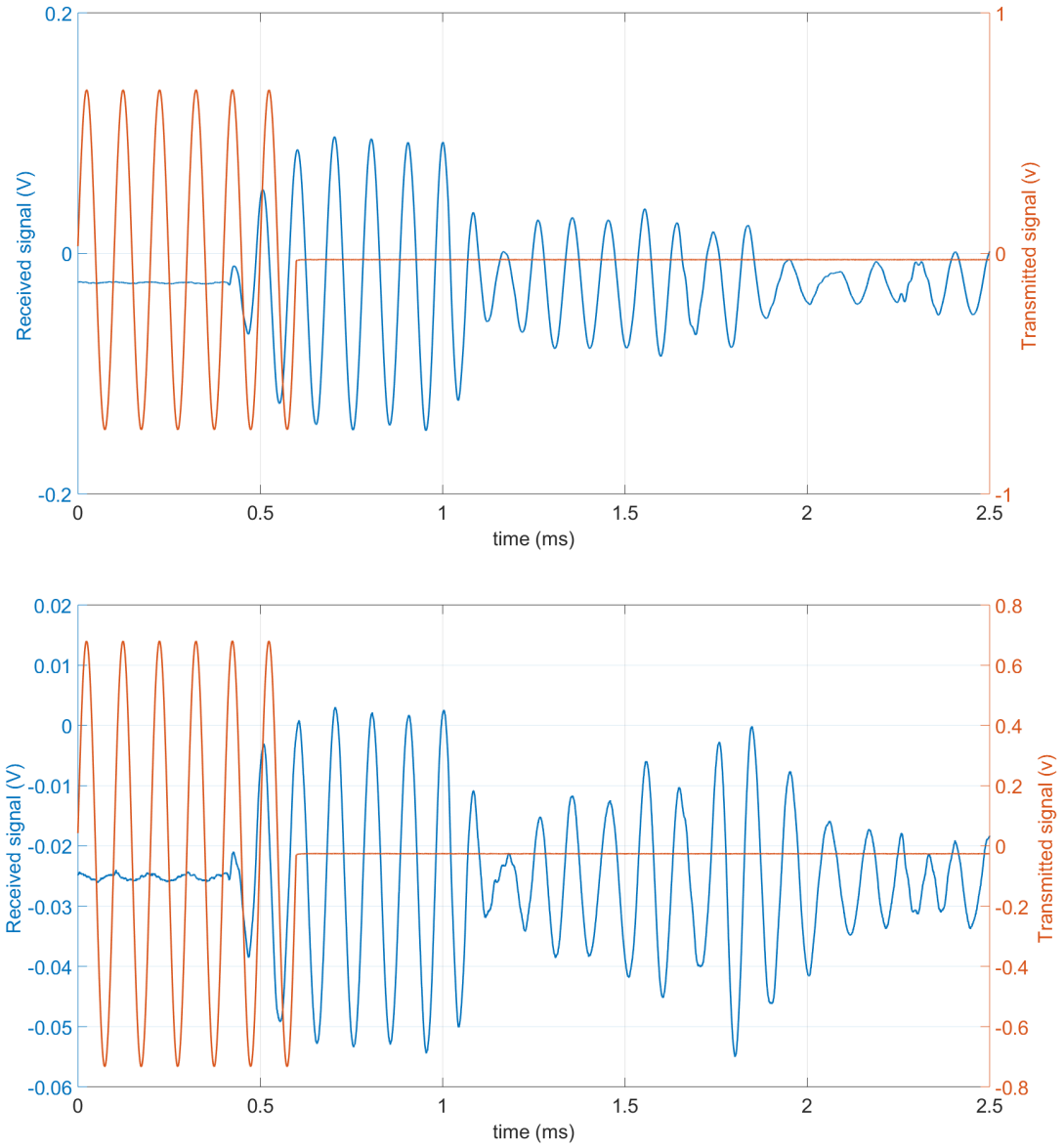

Figure 4.18: Tank experiment using setup TR. The ITC-2044 transmitted 6 cycle long CW pulses at 10 kHz. The red line represents the signal at the output of RP and the blue line represents the signal at the receiver (RESON TC4033). The upper panel shows the signals without bubbles between the transmitter and the receiver, the bottom panel shows the signals when bubbles are released between the transmitter and the receiver.

curves. For the bubble free case it was found 0.2791 ms, corresponding to a distance of 0.4187 m (sound speed 1500 m/s), which is in agreement with the geometry. When bubbles were released between the receivers the travel time was 0.3 ms, corresponding to a sound speed of 1400 m/s.

The attenuation estimated from the measurements for the bubbles free case was 7 dB, in a good agreement with the expected spreading loss, 7.5 dB. The attenuation estimated from the measurements for the bubbles case was about 27 dB, therefore the attenuation due to bubbles is about 20 dB. The larger attenuation and travel time differences observed in this test is in line with the larger flow of bubble.

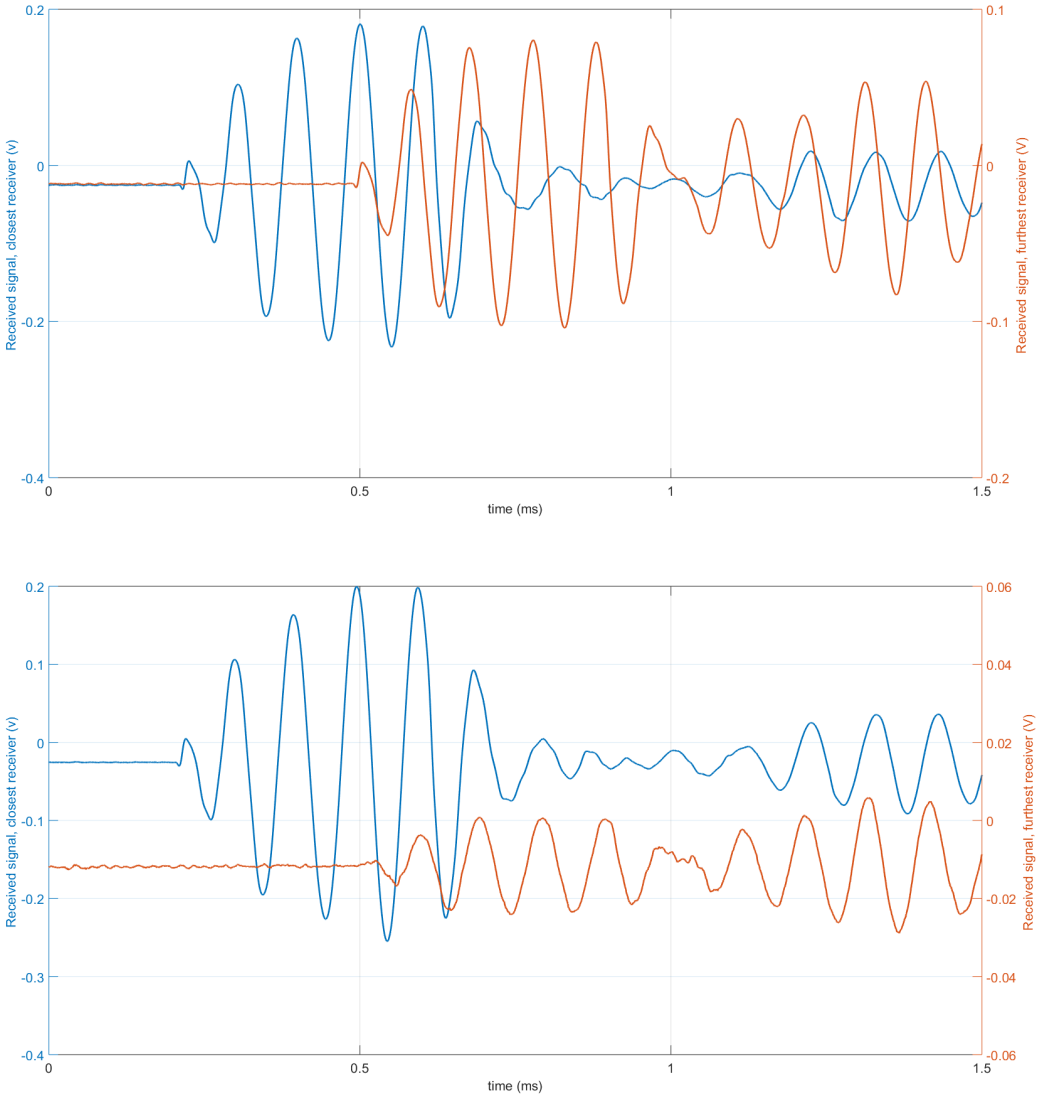

Figure 4.19: Tank experiment using setup TRR. The ITC-2044 transmitted 4 cycle long CW pulses at 10 kHz. The blue line represents the RESON TC4033 closest to ITC-2044, whereas the red line represents the farthest away. The upper panel shows the signals without bubbles between the receivers, the bottom panel show the signals when bubbles are released between the receivers.

The setup TRR is more convenient for travel time and attenuation measurements than setup TR when identical receivers are used because it is not mandatory to accurately know the characteristics of the components in the transmitter chain (amplifier, source, etc). On the other hand, the geometric constraints (distance between the source and the farthest receiver) is more difficult to fulfill in setup TRR, because the constraint given by (3.10) must be verified between the source and the farthest receiver.

4.3.2 Final setup

In the previous section, it was concluded that setup TRR is more efficient for the calculation of signal propagation times. However, the geometry of the setup had to be improved because of problems experienced during field experiments (see Section 5.2.1) so it was decided to build a dedicated structure to hold the hydrophones in fixed position. The structure is entirely constructed of 316 stainless steel in order to resist prolonged submersion and to be resistant to corrosion caused by salt water.

The dimensions of the configuration of the structure are shown in Figure 4.20. Nevertheless, the structure was built to be easily resize the dimensions of the setup. This structure is approximately 1.20 m long, 0.80 m wide at the base and 1.10 m high.

The main purpose of the construction of this structure is to eliminate the small oscillations of the hydrophones, this is, in the previous calibration (shown in Section 4.3.1) the hydrophones are only hanging, which causes oscillations in the hydrophones that may not remain at the ideal and initial distances.

These final calibrations of the system were performed at the Aquaculture Research Station (IPMA-EPPO) of Portuguese Institute for the Sea and Atmosphere, Olhão, southern Portugal, in a tank with nothing inside, besides salt water and air bubbles (the same conditions as the calibration experiment of the primary setup, Section 4.3.1).

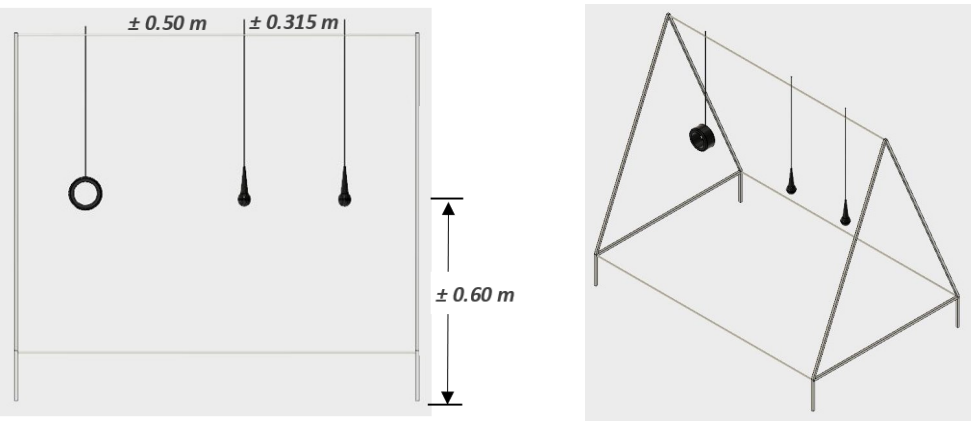

Figure 4.20: Final setup with the hydrophones fixed in the stainless steel structure. The black ring represents the transmitter (transducer ITC2044) and the two black circle represents the two receivers (transducers RESON TC4033).

As in the previous experiments of the primary setups, in this final setup, the same tank was used to perform the setup calibrations. As I mentioned above, the dimensions of the tank are 5 m of length per 2.5 m of width and 1.8 m height (with 1.6 m water depth). The same bubble production mechanisms were used during this experiment (flow is controlled manually but bubble size and flow are unknown).

The structure submerged in the tank with the hydrophones placed according to the setup of Figure 4.20 is shown in Figure 4.21. The bubble diffuser used in the calibration of the system, placed between the two receivers, is also shown in this figure (the long black foam producing bubbles in the right).

Basically, throughout this system calibration experiment were transmitted signals of various frequencies between 4kHz and 20kHz. During the transmissions, the air bubbles were released through the foam diffuser, however, this diffuser creates large bubbles and the flow of bubbles is also quite complicated to be controlled, as stated above. At each frequency, five acquisitions were made and the values of the received signals analyzed later were the values of the third acquisition. The processing of the received signal data was then performed, as discussed in Section 4.2.1. These data are presented in Table 4.8 and 4.9, without and with bubble production, respectively.

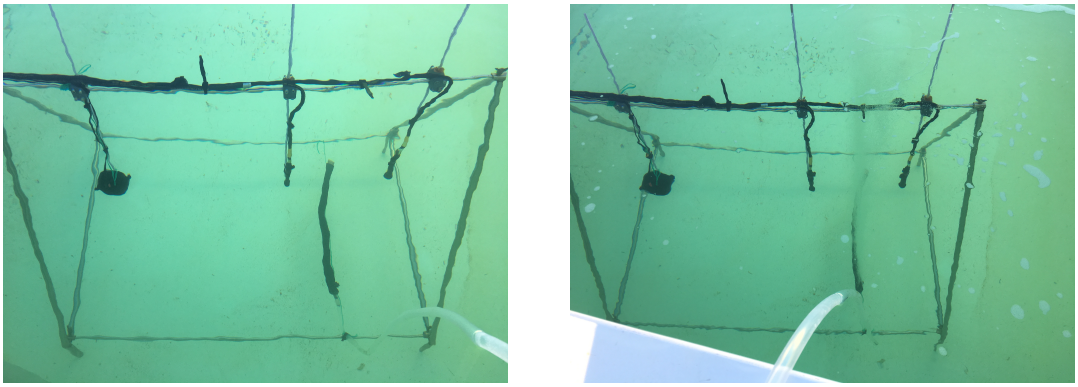

Figure 4.21: Final calibration photos (without bubbles on the left and with bubbles on the right). The bubble diffuser is shown on the right, a long black foam between the two receivers.

In addition, the sound speed in the tank was calculated through the CTD sensor, and it was seen that the sound speed was constant during the experiment, usually 1510 m/s.

Freq [kHz]	**Amp_1 [V]**	**Amp_2 [V]**	**$Time_1$ [ms]**	**$Time_2$ [ms]**	**ssp [m/s]**	**Att [dB]**
4	0.010146	0.0040902	0.30515	0.51098	1530.43	7.89
6	0.028869	0.012134	0.30362	0.51149	1515.36	7.53
7	0.042974	0.018052	0.30362	0.51098	1519.09	7.53
8	0.05895	0.024743	0.3031	0.51098	1515.36	7.54
9	0.075587	0.031421	0.30259	0.51046	1515.36	7.62
10	0.0927	0.038035	0.30208	0.50995	1515.36	7.74
12	0.12299	0.049243	0.30157	0.50944	1515.36	7.95
14	0.13622	0.052701	0.30003	0.5079	1515.36	8.25
16	0.12959	0.047802	0.29798	0.50637	1511.63	8.66
18	0.045332	0.016516	0.23962	0.44698	1519.1	8.77
20	0.04542	0.015872	0.24269	0.44954	1522.86	9.13

Table 4.8: Final calibration table without bubbles

In both tables, the $\mathbf{Amp_1}$ and $\mathbf{Amp_2}$ represents the amplitude of the first peak of the received signal of the first and second receiver. The $\mathbf{Time_1}$ and $\mathbf{Time_2}$ represents the time of the first peak of the received signal of the first and second receiver. The detection of this peak is done as explained in Section 4.2.1 (Peak detection and Measurements).

The **ssp** represents the sound speed profile calculated through the values of the

times of the first peaks of the received signals. The **Att** represents the attenuation of the signal calculated through the values of the amplitudes of the first peaks of the received signals.

The expected attenuation of the signal, only considering the distance between the receivers, approximately 31,5 cm, is about 10 dB (spreading loss).

According to the values of the sound speed in Table 4.8, the value of the sound speed in this frequency range (1515 $\rightarrow$ 1530 m/s) is approximately the same as calculated by CTD ($\pm$ 1510 m/s). The values of the attenuation of the signal vary with the frequency of the signal, however, this variation is not significant. The attenuation is around 8 dB.

Freq [kHz]	**Amp_1 [V]**	**Amp_2 [V]**	**$Time_1$ [ms]**	**$Time_2$ [ms]**	**ssp [m/s]**	**Att [dB]**
4	0.010137	0.0011801	0.30515	0.53299	1382.55	18.68
6	0.028845	0.0035787	0.30362	0.53299	1373.29	18.13
7	0.042839	0.0051164	0.30362	0.53402	1367.19	18.46
8	0.058952	0.0063305	0.3031	0.53248	1373.29	19.38
9	0.075502	0.0058247	0.30208	0.53402	1358.13	22.25
10	0.092618	0.0074433	0.30157	0.53248	1364.16	21.9
12	0.12301	0.0068875	0.30106	0.53043	1373.29	25.04
14	0.13632	0.0075116	0.30003	0.53094	1364.16	25.18
16	0.12947	0.004932	0.2985	0.52685	1379.45	28.38
18	0.045427	0.0016988	0.23962	0.46336	1407.86	28.54
20	0.045435	0.0012743	0.24269	0.46387	1424.15	31.04

Table 4.9: Final calibration table with bubbles

When bubbles were released between the receivers the travel time was increased, corresponding to a decrease of sound speed profile. Depending on the frequency of the signal, this sound speed varies between 1360 and 1420 m/s, approximately. The attenuation estimated from the previous results (without bubbles) was 8 dB. The attenuation estimated from the measurements for the bubbles case, shown in Table 4.9, varies with frequency of the signal between 18 dB and 30 dB, approximately. Therefore the attenuation due to bubbles ranges from 10 dB (lowest frequency) to 22 dB (highest frequency).

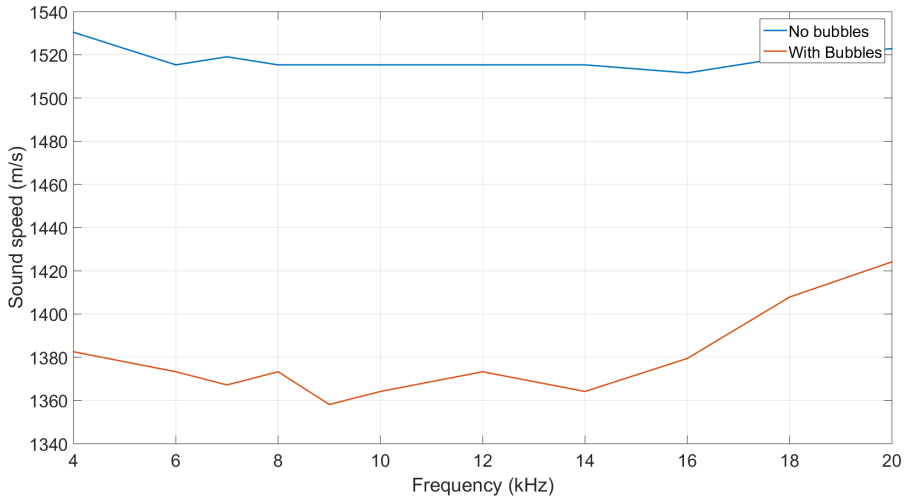

Figure 4.22: Comparison of sound speed when there are no bubbles (blue) and when bubbles are released between the receivers (red).

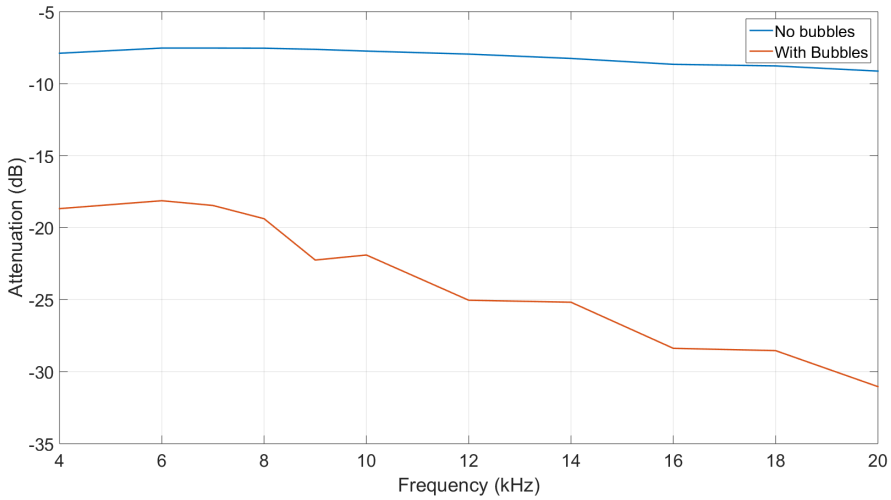

Figure 4.23: Comparison of attenuation of the signal when there are no bubbles (blue) and when bubbles are released between the receivers (red).

In Figure 4.22 is possible to see the variation of the sound speed at each frequency, when there are no bubbles and when bubbles are released between the receivers. It is verified that when there are bubbles the sound speed decrease in all frequencies and this decrease is in order of approximately 140 m/s, which is in line with what is

expected.

In Figure 4.22 is possible to see the variation of the attenuation of the signal at each frequency, when there are no bubbles and when bubbles are released between the receivers. It is verified that, when there are bubbles the attenuation of the signal increase in all frequencies and this increase is in order of 10 dB at low frequencies and 20 dB at high frequencies, which is in line with what is expected.

5

Field Experiments

The development of a measurement system to estimate the oxygen bubbles produced during the photosynthesis of marine plants was discussed in the previous chapter. The proposed system is based on the estimation of the effective sound speed of a bubbly water from the travel time measurements and the attenuation of the propagated signal. Then, the bubble's volume might be estimated from the Wood's equation, shown in equation 3.3.

Throughout the development of the measurement system, several experiments were carried out with the aim to know the environments and know their effects on acoustic propagation. Therefore, in this chapter, will be shown the first approach (preliminary experiments) to verify if there would be the production of bubbles and what

would be this production. Finally, the experiments performed with the developed measurement system will be shown in Section 5.2 (Experiments with the developed system).

5.1 Preliminary experiments

The field experiments were carried at the Aquaculture Research Station (IPMA-EPPO) of Portuguese Institute for the Sea and Atmosphere, Olhão, southern Portugal, in a tank with seagrass and conditions very similar to the conditions in *Ria Formosa*, when the weather conditions favors the bubbles formation by photosynthesis.

The tank used in these preliminary experiments is an open water tank, ie, it is connected through a channel with the *Ria Formosa*. Figure 5.1 shows the location of various tanks and the depth at tank (C), the tank used in these experiments. The tank is covered by marine plants, particularly *Cymodocea nodosa* and *Zostera marina*, however, *Cymodocea nodosa* covers almost completely the tank with few uncovered patches.

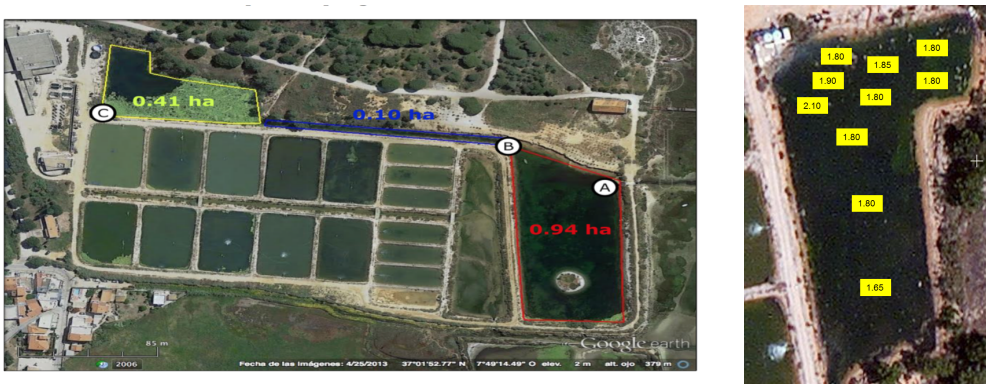

Figure 5.1: Experimental area: EPPO areas with *Cymodocea nodosa* and *Zostera marina* and water depths at the tank labeled (C) (on the right).

The tank (A) is directly connect to the *Ria Formosa* through a gate and the tank (B) is basically a channel between tank (A) and (C). In tank (C) there are pumps to pump the water to other smaller tanks in the research station. The selected tank for this experiment is tank (C) because of the proximity to the pumps station and the possibility of using a support boat. The water depth in the tank is about 1.8 meters

and varies with the tide, ranging from 1.4 to 2.1 m. The main contributions for the acoustic noise of the tank is generated by the water pumps that I already mentioned.

The main purpose of these preliminary experiments is to verify the existence of oxygen bubbles produced by marine plants during the day, particularly due to photosynthesis process. These experiments only had a passive component of the signal, the study being carried out essentially through the ambient noise coming from the water pumps. As I previously stated, at one extremity of the tank (C), there are aeration pumps and water pumps that provide the major part of the ambient noise of the local. When working, aeration pumps produce bubbles, which influences the acoustic signature because attenuate the noise generated by the water pumps.

Figure 5.2: On the left panel, the CTD and SR-1 moorings before deployment. On the right panel, a view of the area from the water pumps control area, showing buoys of the moorings. The white foam is due to aeration pumps.

The equipment used in these experiments was deployed at 20-30m from the water pumps area. Basically, it was used one self-recording hydrophone SR-1 borrowed by *Marsensing* to acquire the ambient noise. The hydrophone was installed at approximately 60cm from the bottom. It was also used the multiparameter CTD RBRconcerto, that in addition to temperature, conductivity and pressure, also measures oxygen concentration.

Two experiments were performed, one with the duration of 2 diurnal periods and

another with the duration of 9 diurnal periods. In the following sections, the two experiments are presented in a more summarized way, the results obtained being shown, although the more detailed results are described in articles (Felisberto et al., 2017a) and (Felisberto et al., 2017b).

5.1.1 July experiment

The experiment carried out during two diurnal cycles from midday of July 25th, 2016 until midday of July 27th, 2016. Was carried out at this season due to the fact that there is a large amount of solar radiation, which causes an increase of the photosynthesis rate and consequent increase of bubble release. The aeration pump was switched off in the fist day, and switched on in the second.

The SR-1 hydrophones recorded 90s snapshots of data at sampling frequency of 52734 Hz, every 10 minutes. The power spectral density of noise was computed using the Welch method from 30s snapshots (last 30s of the .wav files) every 10 minutes using a 2048 points FFT with 512 samples overlapping.

Figure 5.3 shows the power spectral density of the ambient noise along the 2 diurnal periods in the 0-25 kHz band and details of 0-2 kHz (upper-right), 2-7.25 kHz (bottom left) and 7.25-25 kHz (bottom-right) bands, whereas the total power in each band is presented in Figure 5.4. In both figures the O_2 saturation level and water depth are plotted as black and green lines respectively. It can be seen that the attenuation of the ambient noise is high (daylight) when the O_2 saturation level is also high. Although, the periods of low O_2 saturation levels have similar extent and values, the noise power is significantly lower during the second period (about 15 dB). During the second period the aeration pumps moored at a location close to the water pumps and between them and the SR-1 hydrophone were working. The bubbles produced by the aeration pumps most likely attenuates the acoustic noise by the water pumps.

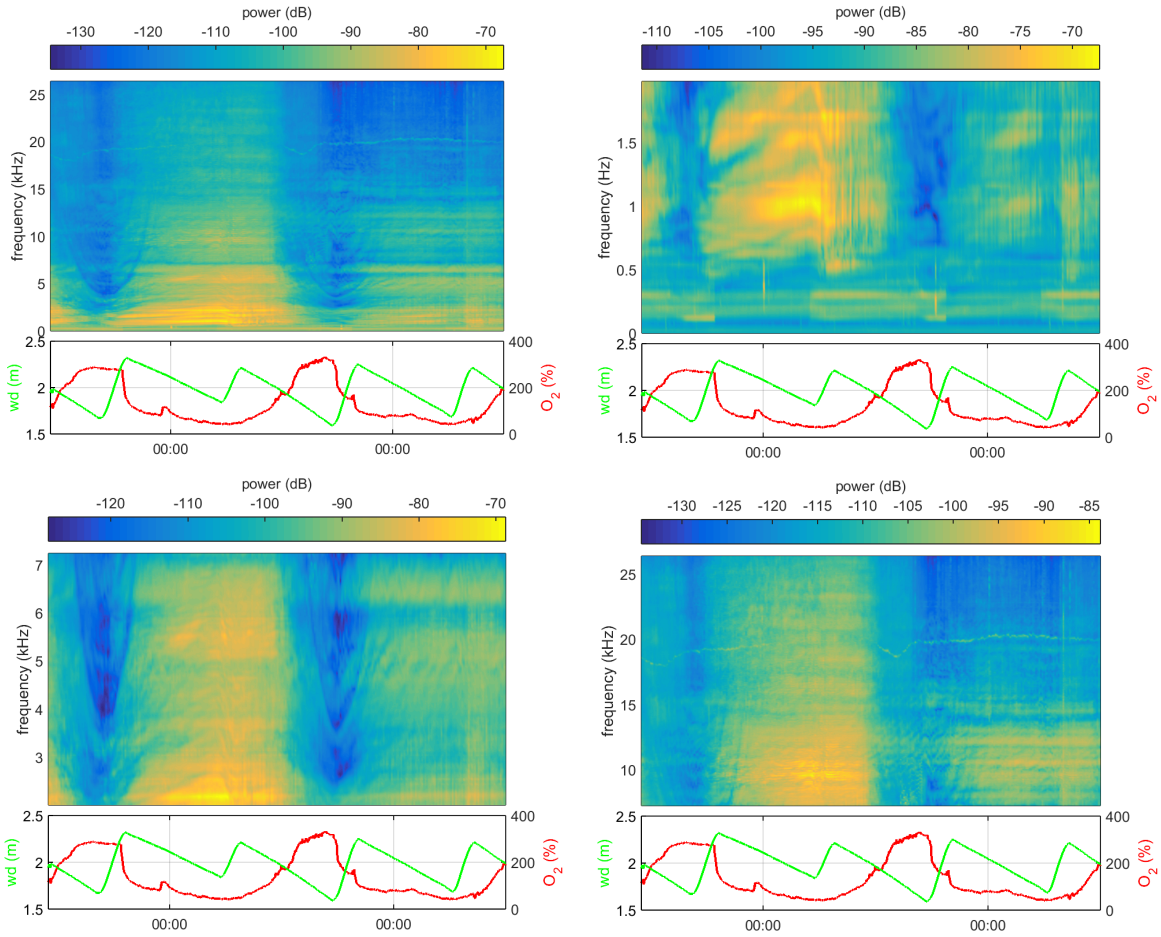

Figure 5.3: Power spectral density of the ambient noise estimated every 10 minutes during 2 diurnal periods: full 0-25 kHz band (upper-left), and zoom of 0-2 kHz (upper-right), 2-7.25 kHz (bottom-left) and 7.25-25 kHz (bottom-right) bands. The red and green curves represent the O_2 saturation and water depth, respectively.

It can be seen, in Figure 5.4, that the attenuation of the ambient noise is high at daylight when the oxygen saturation level is also high, what can be ascribed to bubbles production. Although, the periods of low oxygen saturation levels have similar extent and values, the noise power is significantly lower during the second period (about 15 dB), when the aeration pumps moored at a location close to the water pumps and between them and the SR-1 hydrophone were switched on. The bubbles produced by the aeration pumps most likely attenuates the acoustic noise produced by the water pumps.

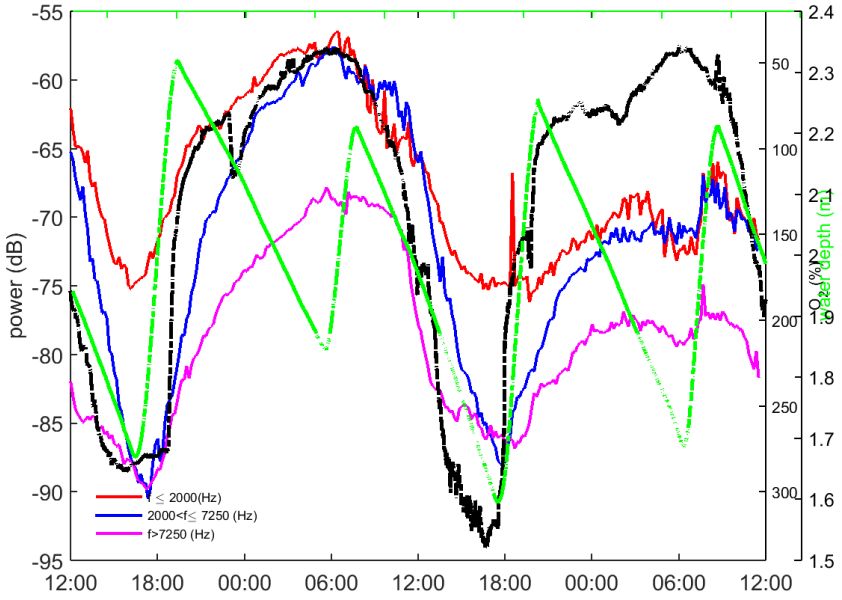

Figure 5.4: Comparison between the variability of the noise power in the bands 0-2 kHz (red), 2-7.25 kHz (blue) and 7.25-25 kHz (magenta), and the variability of O_2 saturation level (black). The green line represents the water depth (estimated from CTD).

5.1.2 October experiment

This experiment was performed from midday of October 11th, 2016 until midday of October 21st, 2016. It is similar to previous experience, but the solar radiation in this season is more weak and the duration of the experiment is longer.

As stated above, the ambient noise is dominated by the water pumps noise and bubbles generated by the aeration pumps attenuate this noise signal. The SR-1 hydrophones recorded 90s snapshots of data at sampling frequency of 52734 Hz, every 10 minutes. The power spectral density of noise was computed using exactly the same procedure described before, in the July experiment.

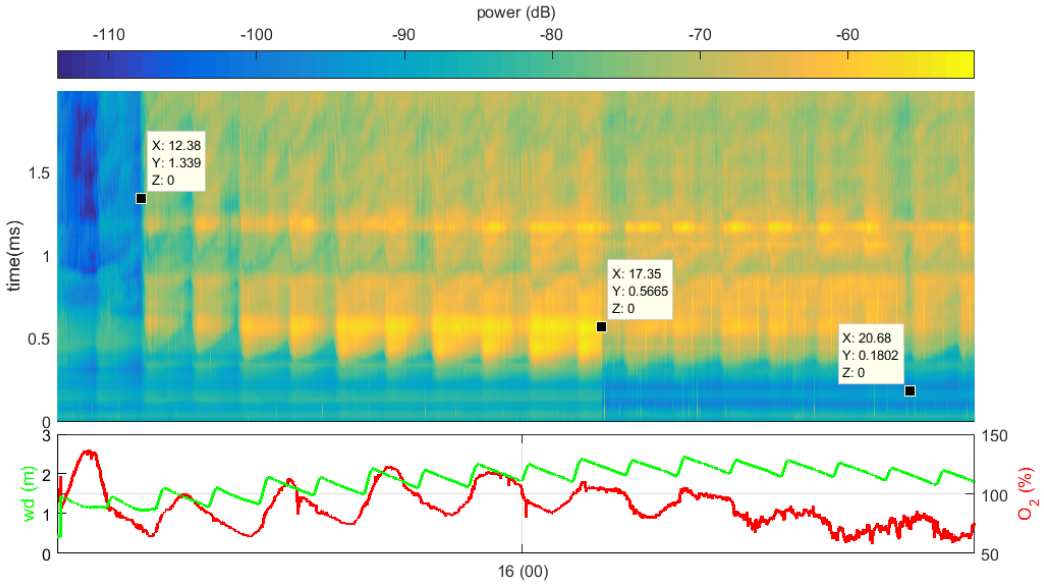

Figure 5.5: Power spectral density of the ambient noise estimated every 10 minutes from October 11th noon until October 20th noon. The red and green curves represent the O_2 saturation level and water depth, respectively. The labels indicates when the aeration pump (1st label) and water pumps were switched off.

Figure 5.5 shows the power spectral density in the 0-25 kHz band of the ambient noise along 9 diurnal periods. In both figures the O_2 saturation level and water depth are plotted as black and green lines respectively. During the period several events significantly affected the measured power of the ambient noise. On October 12th at 9 am the aeration pump was switched off, giving rise to a significant increase of the noise power at the hydrophone. On October 17th at 9 am and on October 20th at 4 pm water pumps were switched off giving rise to a decrease of ambient noise.

Figure 5.6 shows the noise power in various frequency bands. The red line represents the lowest band (0-2 kHz), the middle band (2-7.25 kHz) is given by the blue line, and the highest band (7.25-25 kHz) by the magenta line. The pumps switch off events are clear seen in the Figure 5.6, where sudden changes in noise power occur at all frequency bands. Apart of this, one can notice the influence of the water depth

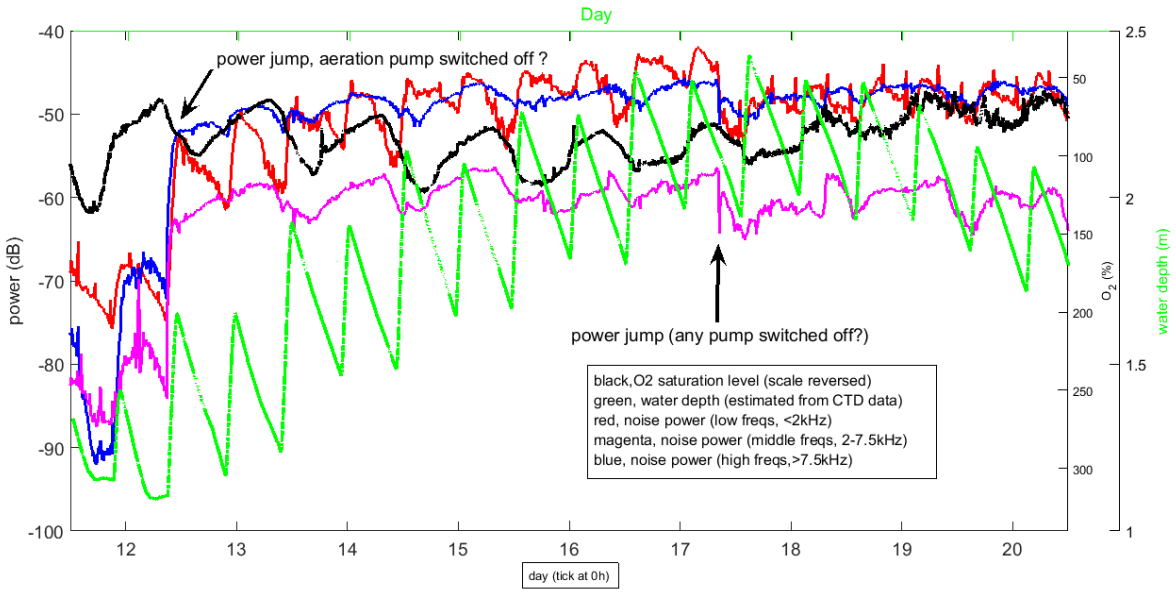

Figure 5.6: Comparison between the variability of the noise power in the bands 0-2 kHz (red), 2-7.25 kHz (blue) and 7.25-25 kHz (magenta), and the variability of O_2 saturation level (black). The green line represents the water depth (estimated from CTD).

variability on the power variability of the lowest frequency band. In the middle and high frequency bands the noise power shows a diurnal change, that may be linked with the photosynthetic activity of the plants.

These experiments show that the photosynthetic activity of seagrass meadow under oxygen supersaturation conditions significantly affects acoustic propagation, probably due to existence of oxygen bubbles. In general, an excess attenuation was observed when the oxygen saturation level is high, what can be ascribed to bubbles production. For frequencies above 2kHz, the variability of the noise power is correlated with dissolved oxygen. In the lower frequencies the variability of the noise power is directly correlated with the water depth.

5.2 Experiments with the developed system

Two experiments were performed using the developed measurement system. One of the experiments was performed in tank (C) (previously shown in Figure 5.1). This experiment has shown some unreliable results (see below) leading to the development of the fixing structure described in Section 4.3.2 (shown in Figure 4.20), and additional experiments performed in the small ground tank with that structure.

The first experiment was carried out in real time, ie, the equipment was placed in the tank and the signals received by the transducers were monitored and recorded. The other experiment was carried out with the duration of two days and a half, approximately, ie, the equipment was placed in the tank to be transmitted signals through the emitter and to record the received signals during this period of time.

The equipment used in these experiments was the developed measurement system. In the first experiment the transducers were placed on a float and in the final experiment the transducers were placed in the stainless steel structure shown in Figure 4.20. In the final experiment, it were also used the ABS and the multiparameter CTD RBRconcerto, that in addition to temperature, conductivity and pressure, also measures oxygen concentration.

5.2.1 First experiment

The experiment was performed on June 9^{th}, 2017, during the period of the morning. Was carried out at this season due to the fact that there is a large amount of solar radiation, which causes an increase of the photosynthesis rate and consequent increase of bubble release.

Basically, this experiment was carried out in the same way as described in Section 4.3.1, however, the geometry had to be adjusted.

The setup TRR was used (see in Figure 4.17) with some geometrical differences. The distance between the two receivers is about 35 cm and the distance from the trans-

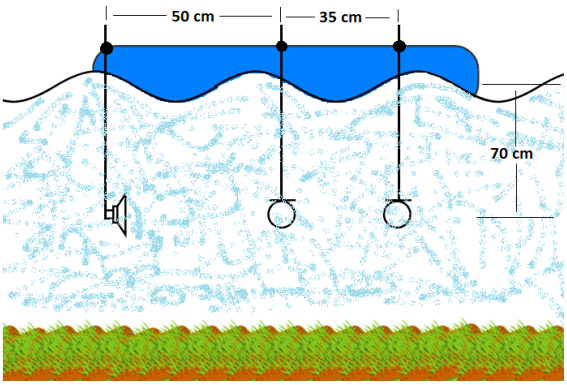

Figure 5.7: Schematic of the float assembly.

mitter to the first receiver is approximately 50 cm. The hydrophones were hung on a float about 70cm from the surface, as shown in Figure 5.7. The float has approximately 100 cm of length and is formed by two equal floats placed side-by-side to give stability to the structure, as shown in Figure 5.8.

The local of the experiment is the tank (C), previously described in Section 5.1, with a high concentration of marine plants, particularly *Cymodocea nodosa* and *Zostera marina*. A small boat was used to support the experiment. The system installed on the float is shown in the underwater photo in the Figure 5.9.

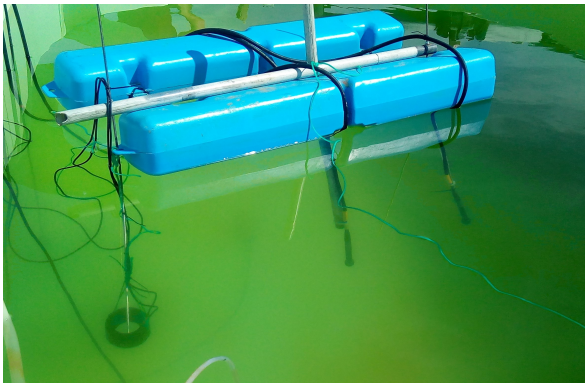

Figure 5.8: Float with the hydrophones in the configuration described in Section 5.7.

The major purpose of this experiment is to measure the propagation times of the signal between the two receivers. The distances between the receivers are known and the system is synchronized, so it is easy to measure the propagation times and estimate the speed of sound in the water column.

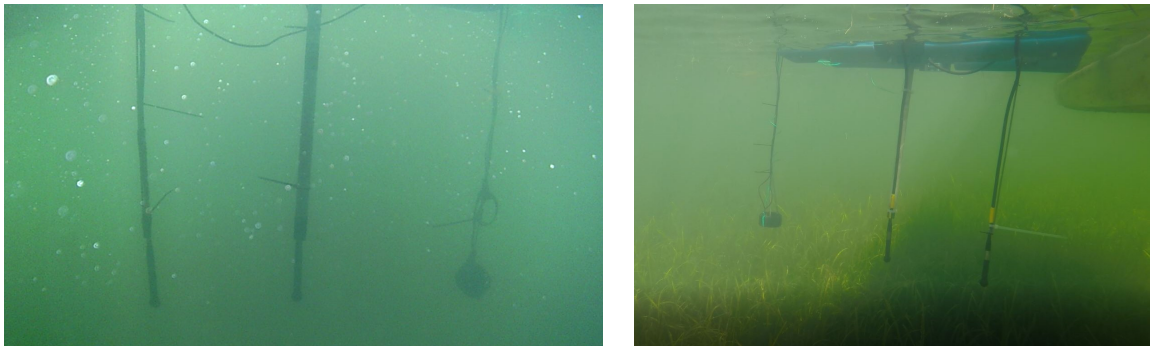

Figure 5.9: Underwater photographies of the system mount. The hydrophone transmitter (ITC-2044) is on the right, the first receiver on the centre and the second receiver on the left (figure on the left).

In Figure 5.10 is shown the signal transmitted by the ITC-2044 with 4 cycle long CW pulse at 10 kHz. The signal acquired by the closest receiver to the transmitter is shown as a blue line, whereas the signal acquired by the receiver farthest away from the transmitter is shown as a red line. Several echoes of the CW pulses can be observed but the only considered is the first echo at the receivers that represents the direct path. Therefore, only the signal up to 2.0 *ms* was considered.

By analysing the peaks of the received signals, were recorded the values of the time and the amplitude of these signals. At the time of this experiment, the peak detection software (shown in Section 4.2.1) was not yet completed, therefore, in this experiment were considered the first peak and the highest peak of each signal.

Considering the values in the Table 5.1, it is possible to calculate the propagation time between the signals, making the difference between the values of the same peaks of the closest receiver signal and of the furthest receiver signal. For example, consid-

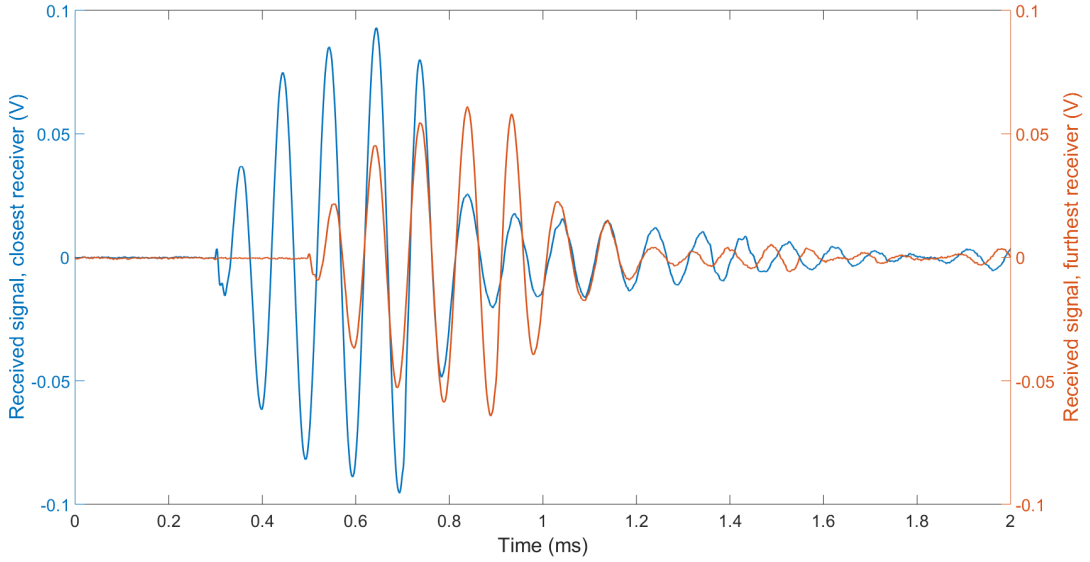

Figure 5.10: Tank experiment using setup TRR. The ITC-2044 transmitted 4 cycle long CW pulses at 10 kHz. The blue line represents the RESON TC4033 closest to ITC-2044, whereas the red line represents the farthest away.

Point	Time (ms)	Amplitude of signal (V)
1st Peak	0.3558	0.03676
4th Peak (highest peak)	0.6436	0.09292
1st Peak	0.5555	0.02162
4th Peak (highest peak)	0.8387	0.06103

Table 5.1: Measures of the values of Figure 5.10. Values of the closest receiver (on the top) and furthest receiver (on the bottom).

ering the highest peak of the signals:

$$Time\ \ propagation = 0.8387 - 0.6436 = 0.1951\ \ ms \tag{5.1}$$

As stated above, the distance between receivers is about 35 cm, therefore:

$$Sound\ \ speed = \frac{distance\ \ (m)}{Time\ \ propagation} = \frac{0.35}{0.1951 \times 10^{-3}} \approx 1793.95\ \ m/s \tag{5.2}$$

On the other hand, it is possible to calculate the attenuation of the signal between the two transducers, according to the values of amplitudes of the same peaks, that is:

$$Att = -20 \times log \frac{amplitude_{\text{peak}_2} \ (V)}{amplitude_{\text{peak}_1} \ (V)} \ [dB] = -20 \times log \frac{0.06103}{0.09292} \approx 3.7 \ dB \qquad (5.3)$$

The values of the first peak were also considered and the propagation times and the attenuation of the signal were calculated with these values, however, the results obtained were practically the same as with the highest peak.

In Figure 5.11 is shown the signal transmitted by the ITC-2044 with 4 cycle long CW pulse at 15 kHz. The signal acquired by the closest receiver to the transmitter is shown as a blue line, whereas the signal acquired by the receiver farthest away from the transmitter is shown as a red line. Several echoes of the CW pulses can be observed but the only considered is the first echo at the receivers that represents the direct path. Therefore, only the signal up to 1.6 *ms* was considered.

Point	**Time (*ms*)**	**Amplitude of signal (*V*)**
1st Peak	0.3579	0.03097
2nd Peak (highest peak)	0.425	0.05269
1st Peak	0.5565	0.01829
2nd Peak (highest peak)	0.6257	0.02943

Table 5.2: Measures of the values of Figure 5.11. Values of the closest receiver (on the top) and furthest receiver (on the bottom).

Through the values in Table 5.2, it is possible to calculate the propagation time between the signals in the same way as in the previous example. Again, in this case, for example considering the highest peak of the signals:

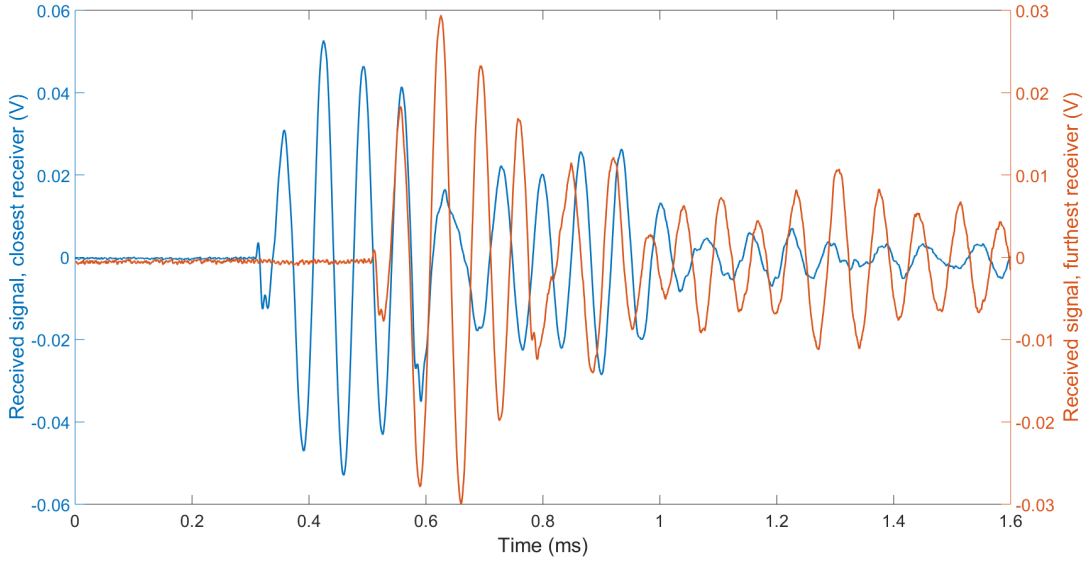

Figure 5.11: Tank experiment using setup TRR. The ITC-2044 transmitted 4 cycle long CW pulses at 15 kHz. The blue line represents the RESON TC4033 closest to ITC-2044, whereas the red line represents the farthest away.

$$Time\ \ propagation = 0.6257 - 0.425 = 0.2007\ \ ms \tag{5.4}$$

As stated above, the distance between receivers is about 35 cm, therefore:

$$Sound\ \ speed = \frac{distance\ \ (m)}{Time\ \ propagation} = \frac{0.35}{0.2007 \times 10^{-3}} \approx 1743,9\ \ m/s \tag{5.5}$$

As in the previous example, it is possible to calculate the attenuation of the signal between the two transducers, according to the values of amplitudes of the same peaks, that is:

$$Att = -20 \times log\frac{amplitude_{\text{peak}_2}\ \ (V)}{amplitude_{\text{peak}_1}\ \ (V)}\ \ [dB] = -20 \times log\frac{0.02943}{0.05269} \approx 5.1\ \ dB \tag{5.6}$$

On average, the sound speed in bubbles free water is about 1500 *m/s* and the factors that effect this are temperature, depth and pressure. In the conditions of the experiments there are no great differences that justify such a high sound velocity.

A possible explanation for this event is that the transmitted signal frequency is very close to the bubbles resonant frequency (Terrill & Melville, 2000), however, the results of the attenuation of the signal do not support this theory. If the value of the sound speed were high because of the frequency of the transmitted signal, the values of the attenuation would have to be greater than at least 9 dB (expected attenuation of the signal, only considering the distance between the transducers, approximately 35 cm).

The geometries of the system assembly may not be the most appropriate for existing conditions, however, these restrictions do not appear to be causing this discovered problem. The only possible explanation, however, may not be the most correct, is due to fact that the propagation of the signal may be occurring by the structure, this is, the signal can be transmitted more quickly by the float structure (insulation problem of the structure). Another hypothesis for the explanation of this problem may be due to constructive interference. This interference may be occurring due to possible reflections in the structure, in this case, the reflections in the rods that hold the transducers.

As this experiment gave rise to several problems, some of which did not know their origin or explanation, was decided to proceed with the construction of the stainless steel structure, shown in Figure 4.20, with the purpose of trying to eliminate some of the possible causes of the problem found in this experiment.

5.2.2 Final experiment

The experiment carried out during two and a half diurnal cycles from morning of November 30th, 2017 until afternoon of December 2nd, 2017. In this experiment was used the system developed throughout this thesis and the installation and operation of the system are exactly as described in previously experiment shown in Section 4.3.2.

The setup TRR depicted in Figure 4.20 was used for data acquisition. The experiment was performed in the ground tank with 5 m of length per 2.5 m of width and 1.8 m height and was used the stainless steel structure to hold the hydrophones.

In this experiment was used marine plants inside the tank so that the production of bubbles is more natural and only depends on the production of the plant. Therefore, was done a transplant of marine plants existing in tank (C), as shown in Figure 5.1. This transplant was carried out with the intention of forming in the small ground tank an environment similar to the one existing in tank (C). Thus, it was possible to make simulations with the system inside a tank with smaller dimensions and with greater ease of access and operability.

Figure 5.12: Transplant of the marine plants using the one shovel (on the left) and placement of the box inside the tank (on the right).

This process was carried out by colleague *André Silva* from Centre of Marine Sciences (CCMAR) of the University of the Algarve. Basically, marine plants with the rhizome were removed with the help of the one shovel. Several pieces of the bottom were picked to the inside of a box so as to have a high concentration of marine plants, as shown in Figure 5.12. This operation took about 10 minutes since the plants were withdrawn from the tank until they were put back into the water. The transplanted marine plants were essentially of the species *Cymodocea nodosa*, however, it is possible to be mixed in the box some plant of the species *Zostera marina*.

The box with the marine plants was placed inside the tank in the area between the two receivers so that the bubbles produced by the marine plants affects only the acoustic signal between the two receivers (see Figure 5.13).

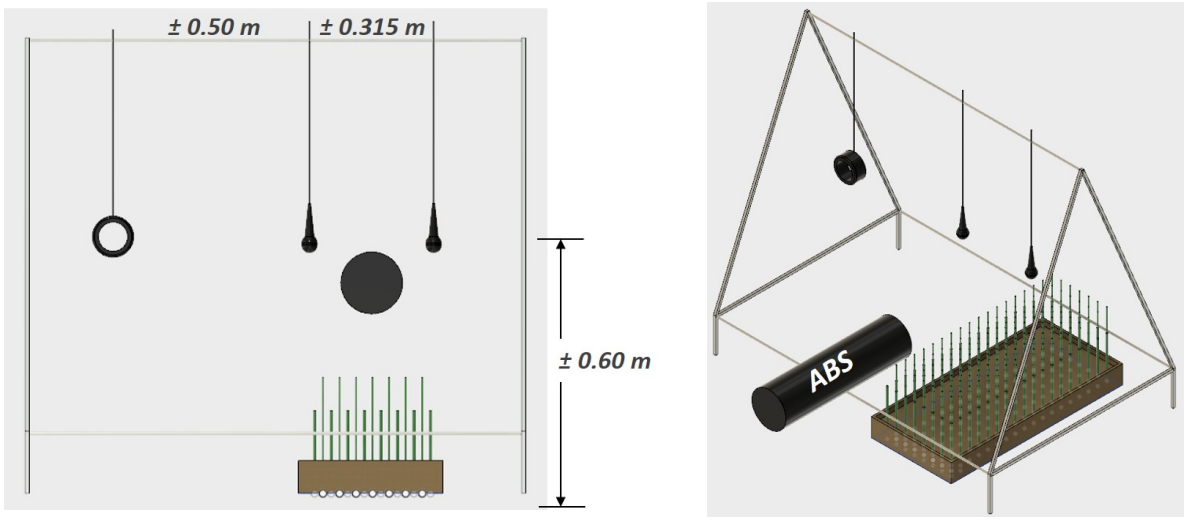

Figure 5.13: Configuration of the final experiment with the placement of the ABS (black circle on the left figure) pointed to the area of occurrence of bubbles produced by the marine plants.

The water in the tank is constantly renewed. A small amount of water is released out of the tank and a small amount of water from tank (C) enters, constantly. This cycle is very important for the survival of the marine plants present inside the box. Plants are expected to be able to live up to 3 weeks under these conditions.

As this experiment was conducted during the Autumn/Winter and the production

of the oxygen by marine plants is lower than in other seasons, it was found necessary to use the ABS (Acoustic Backscatter System) to monitor the presence or absence of bubbles during the peak of production of the oxygen. The ABS operates at high frequencies (0.5 - 4 MHz), basically, the system sends the signal and the bubble works as a barrier, gives it back the signal with different values of power, so it is possible to check for bubbles or not in a specific area. As shown in Figure 5.13, the ABS is pointed to the area of occurrence of bubbles produced by marine plants at a distance of 0.50 m from the bottom and about 0.30/0.40 m from the plant area, approximately. The box where the marine plants were placed is about 0.8 m of length and 0.4 m of width, covering a total area of approximately 0.32 square meters (m^2).

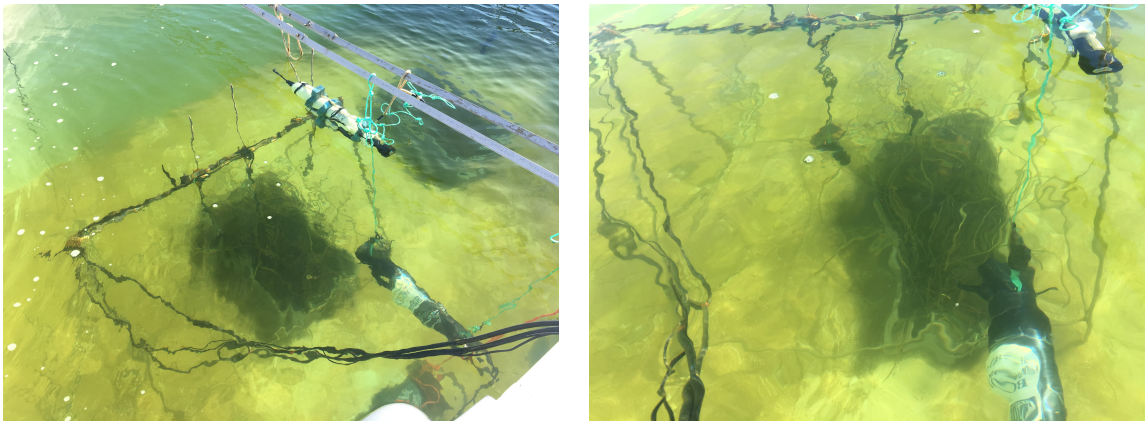

Figure 5.14: Equipment placed inside the tank. Hydrophones mounted on the structure, the box with marine plants on the bottom and the ABS (black cylinder) and the CTD (white cylinder) suspended by a rope.

After the box with the plants was placed inside the tank, the plants were straightened by hand so that they were stretched along the water column.

Other complementary measures were also performed using the multiparameter CTD RBRconcerto with an optode to measure the oxygen. This equipment collected pressure, depth (in this case is constant, tank depth is about 1.60 m), conductivity, temperature and dissolved O_2 data at sampling frequency of 1 sample every 5 minutes. As shown in Figure 5.14, the CTD (in figure, is the white cylinder suspended by green ropes) was placed above the plants area and the ABS (in figure, is the black cylinder)

was placed pointed at the plants area, as already mentioned above.

In addiction, the meteorological data, provided by EPPO-IPMA, were recorded every 10 minutes by a meteo station installed in top of a station building. This meteo station measures a lot of parameter, however, the solar irradiance is the most relevant parameter for the photosynthetic activity of the plants because it measures light availability, however, the wavelength is not known.

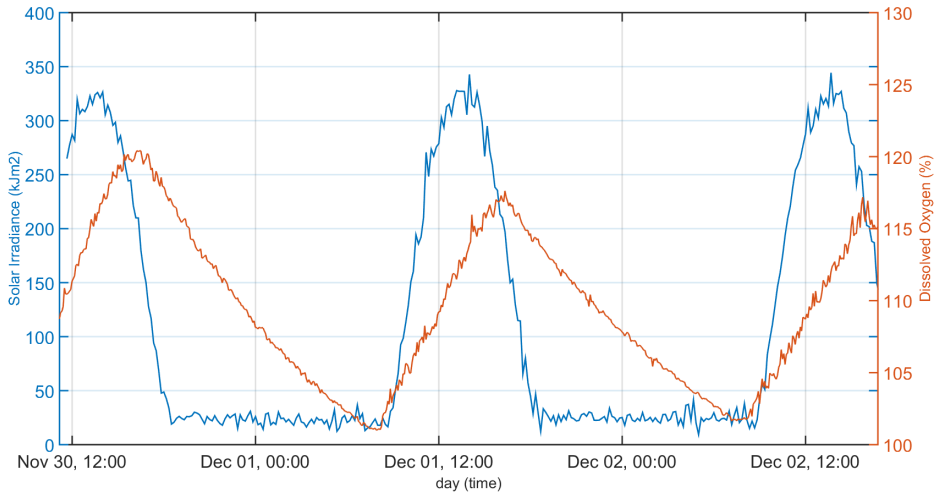

Figure 5.15: Relation between the solar irradiance (blue) and the dissolved oxygen (red) in the water inside the ground tank.

It can be seen, in Figure 5.15, that there is a correlation between the solar irradiance and the dissolved oxygen in the water column, as expected. The solar irradiance has practically the same peak values during the days of the experiment, and these peaks occur between 12 pm and 14 pm, approximately. During the period of the day, the dissolved oxygen has a higher value compared to the night period, which suggests that the marine plants are correctly performing the photosynthesis process. The dissolved oxygen shows a diurnal pattern with a minimum at 8 am, then increases until 16 pm, approximately. After this instant of time, the dissolved O_2 decreases more slowly until 8 am, night period. The saturation level reaches a maximum of approximately 120 % in the 1^{st} daily cycle and 115 % in the following cycles. These results suggest that there is bubble production in the water column because there is supersaturation (above $\pm$

100%).

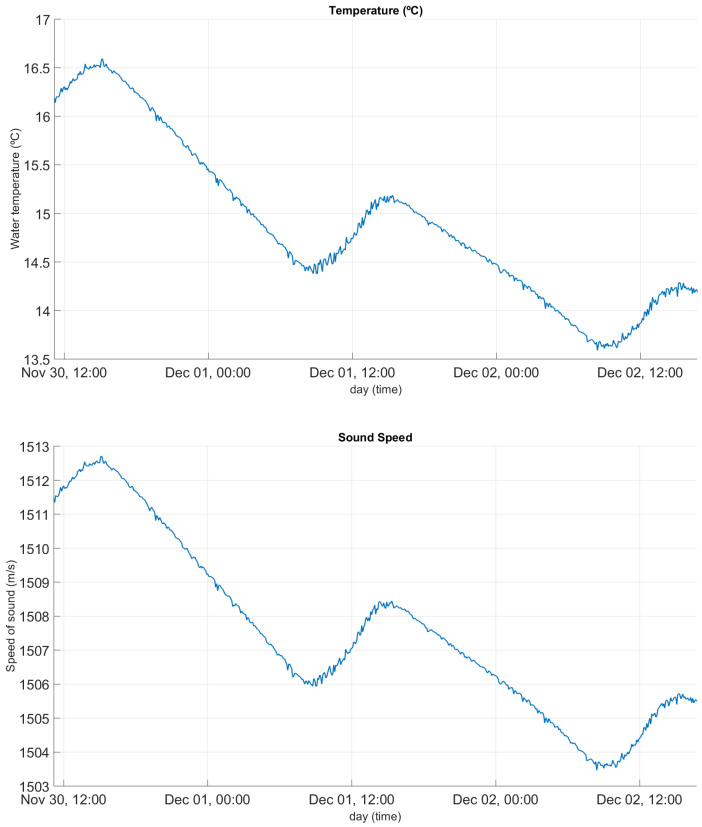

Figure 5.16: CTD data: Water temperature (upper) and Sound speed (bottom).

The water temperature and sound speed data are presented in Figure 5.16. The water temperature varies about 2°C during the first period and 1.5°C during the second period, showing a pattern in both periods. These patterns are correlated with the dissolved oxygen patterns.

The sound speed varies between 1506 and 1512.5 m/s during the first period and between 1503.5 and 1508.5 m/s during the second period, and as expected follows a pattern similar to the temperature. Several authors correlate the two parameters, concluding that the 1°C increase in temperature increases the sound speed in 3 m/s, approximately, which is in accordance with the data measured by the multiparameter CTD.

As stated above, the ABS was only used to check for the occurrence of bubbles pro-

duced by marine plants. Sequences of backscatter data were acquired every 5 minutes during the experiment period.

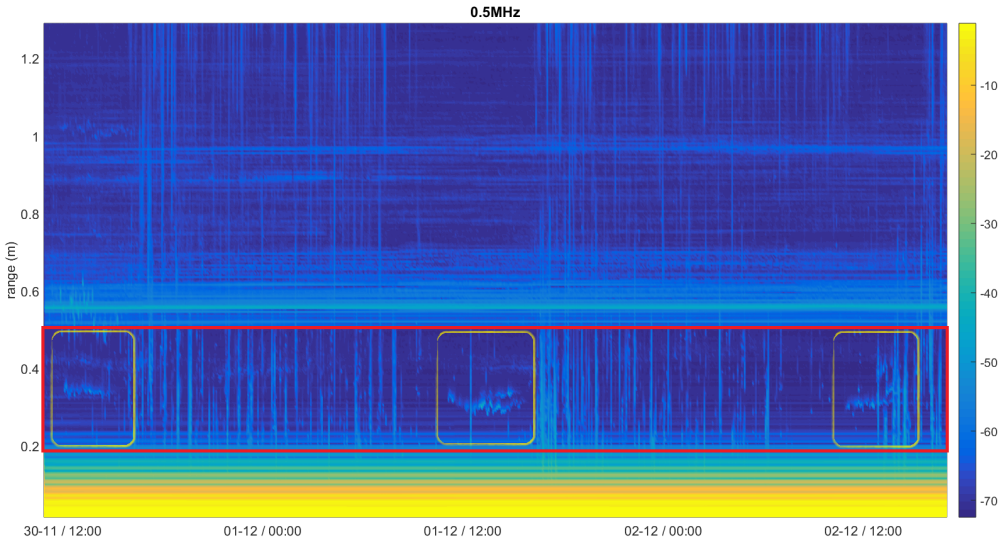

Figure 5.17: Backscatter level measure by the ABS at 0.5 MHz sensor during the experiment period. The red rectangle represents the marine plants area. The yellow rectangle shows the scatters (suggest bubbles) during the period of the day.

Figure 5.17 shows the backscatter level measured by the sensor of 0.5 MHz. Its possible to see when the O_2 saturation level is high, during the period of the day, the occurrence of the scatters in the area where marine plants were placed. These phenomena occurs throughout the periods of the day during the two and a half days, and these periods are represented by the yellow rectangles. The area above the area where plants were placed are represented by the red rectangle.

These scatters may suggest that there are bubbles released by the plants along the water column in this area. However, the level of the scattered signal in this area is not very high because the production of bubbles is low due to the fact that the experiment was carried out in the Autumn/Winter. Compared with previous experiments performed in the Summer (e.g. see Section 5.1.1), oxygen production and bubble formation by marine plants is much lower at this time. It can also be seen at approximately 0.55 meters from the sensor, a constant scatter over time. This is due to the fact that

the sensor of the ABS may be pe pointing slightly towards the transducer, causing this reflection. This scatter may be parts of the structure too.

It can be seen, in Figure 5.18 the zoom of the red rectangle area of the Figure 5.17, i.e., only the backscatter level measured in the area above where the marine plants were placed. Once again, the scatters are visible in the spectrogram during the period of the day when there is a greater production of oxygen, and therefore there is the occurrence of bubbles in the water column (as shown in Figure 5.18 at the yellow circles). These scatters appears between 0.30 and 0.40 meters of the sensor, so, are exactly in the area above the plants, which proves the appearance of the oxygen bubbles. The constant lines that appear most often during the period of the night, and are present over the entire width of the tank, is just noise in the tank.

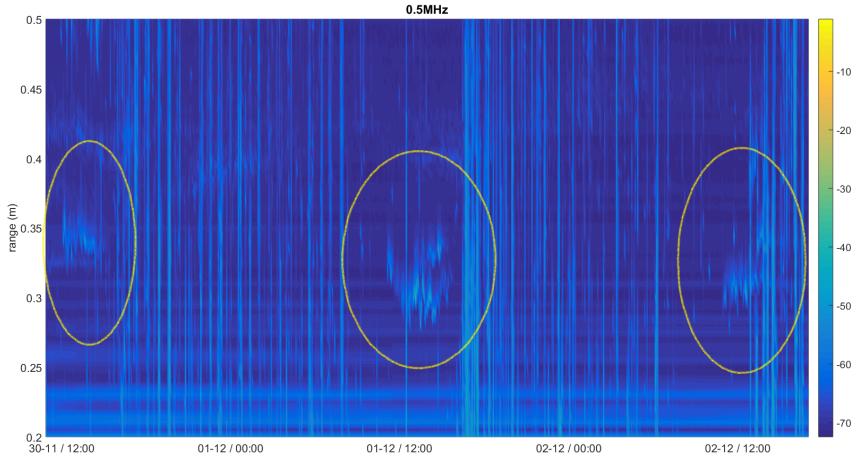

Figure 5.18: Backscatter level measured only in the area above where the marine plants were placed. The yellow circles shows the scatters during the period of the day.

As I stated above, was used setup TRR with the developed measurement system, and were transmitted various sequences of signals from 4 to 20 KHz, as shown in Section 4.2. These sequences were transmitted and acquired during the experiment period with a pause interval of approximately 15 minutes between each sequence. In each sequence, are acquired five signals per each frequency. Then, in processing the data, was calculated the mean between the five signals. The considered time of the signal of each frequency is the time of the third signal. After the acquisitions were

completed, was performed the peak detection of all data, as shown in Section 4.2.1, and after that, were calculated the sound speed and attenuation of the signal.

The sound speed measured by this method, compared to the sound speed measured by the CTD (see in Figure 5.16 on the bottom), follows the similar pattern, however, the peaks of sound speed are in line with the peaks of oxygen.

When there are few bubbles, as in this case, it is difficult to estimate the propagation times because the temperature becomes a strong factor for this measurement, ie, the component of variation due to temperature is much larger than the effect due to bubbles.

It was expected that the sound speed decreases during the oxygen peaks due to the presence of the bubbles, which happening exactly the opposite. This fact may be due to the frequency of the signal may be close to the resonance frequency.

At 6 kHz the sound speed has a maximum peak during the first period of the day of about 1535 m/s and decreases until about 1507 m/s during the first night. The second period of the day has a maximum peak of 1520 m/s and after, decrease until 1507 m/s, approximately. In the case of 10 kHz signal, the maximum peak during the first period of the day is about 1522 m/s and decreases until about 1505 m/s, and the second period of the day has a maximum at approximately 1514 m/s and after then a minimum at 1504 m/s. At 15 kHz the sound speed vary between 1515 and 1501 m/s during the first experiment day and very between 1507 and 1498 m/s during the second period.

Freq [kHz]	**Max1 [m/s]**	**Min1 [m/s]**	**Max2 [m/s]**	**Min2 [m/s]**
6	1535	1507	1520	1507
10	1522	1505	1514	1504
15	1515	1501	1507	1498
CTD	1512.5	1506	1508.5	1503.5

Table 5.3: Comparison between sound speed measured by the CTD and the sound speed measured by the travel time measurement. Data from the Figure 5.19.

The measurement data shows that sound speed increase during the period when

there is greater production of the oxygen and bubbles in water column. This fact was not expected, because normally when there is an existence of bubbles, the sound speed decreases, as previously shown in Section 4.3.2. However, the only possible explanation is that as the production of bubbles is weak, the main factor influencing the speed of sound is temperature. Basically, in this scenario, is difficult to estimate the production of bubbles through the sound speed.

In Figures 5.20 and 5.21 are shown the values of the attenuation of the signal between the two receivers and additionally the value of the dissolved oxygen measured by the CTD placed above the marine plants. In both frequency analyzed, the signal attenuation follows the pattern of the dissolved oxygen, i.e., when there is an increase in dissolved oxygen, during the period of the day, there is also an increase in attenuation of the signal. Otherwise, when the dissolved oxygen level is low, the attenuation of the signal is low too. This fact can easily be explained by the existence of oxygen bubbles released by the marine plants during the period of solar exposure, due to photosynthesis.

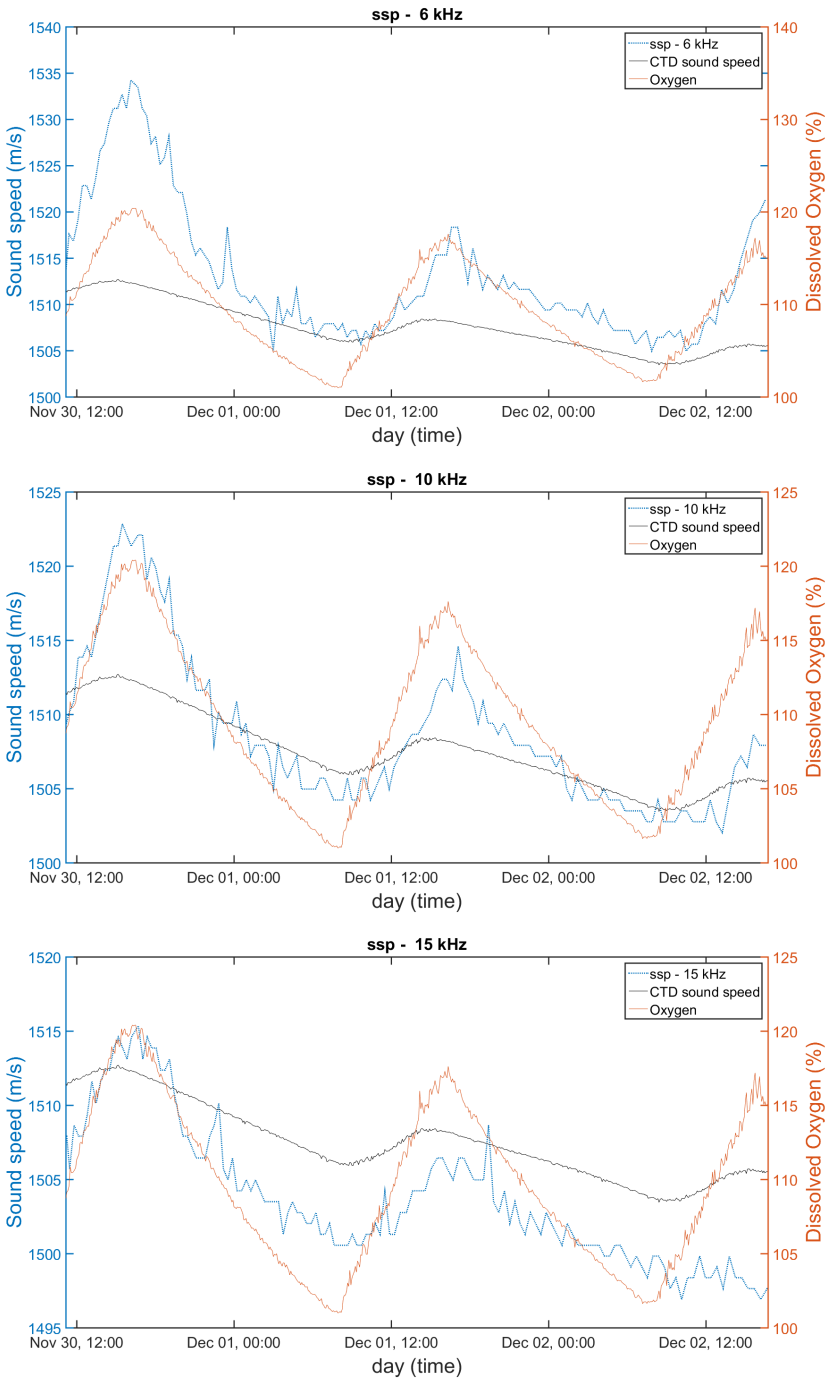

Figure 5.19: The comparison between the sound speed measured by the CTD (black) and the sound speed according to short range propagation and the measurement system explained in Chapter 4 (blue), for signals transmitted at 6 kHz (on the top), 10 kHz (on the middle) and 15 kHz (on the bottom). The oxygen dissolved during the experiment period is shown in red.

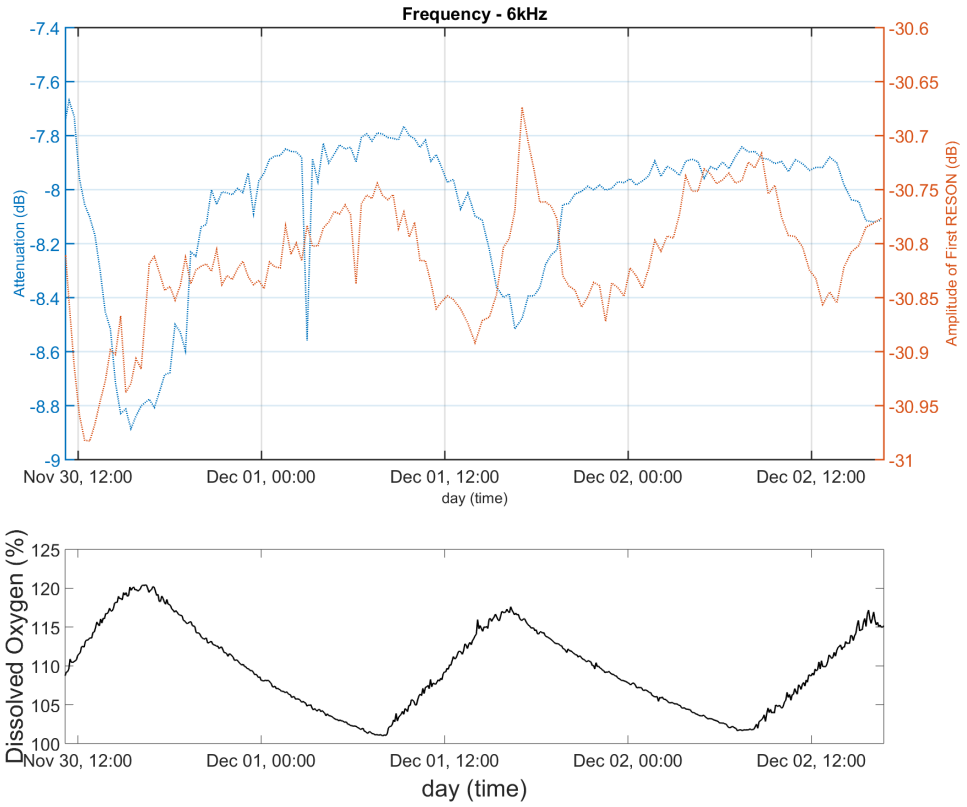

Figure 5.20: At the top, the comparison of the signal attenuation between two receivers (blue) and the amplitude of the signal received by the first receiver, closer to the source (red), for signals transmitted at 6 kHz. At the bottom, the oxygen dissolved during the experiment period (black).

In both figures is also shown the power of the amplitudes of the first receiver over time. This measure is a complement to prove that attenuation of the signal is essentially due to oxygen bubbles produced by marine plants, because in the area between the transmitter and the first receiver there are no marine plants in the bottom, so in principle, there will be no bubbles in the water column in that zone.

At 6 kHz, as shown in Figure 5.20, the attenuation of the signal increase in about 1.1 dB during the first peak of dissolved oxygen ($\pm$ 120 %) to values close to 8.9 dB and during the first period of the night the values of attenuation is 7.8 dB, approximately. In the second period with more intensity of sunlight ($\pm$ 118 %), the attenuation of the signal has increased 0.7 dB to a total of 8.5 dB. On the other hand, the amplitude of the first receiver during the first peak of dissolved oxygen increase only $\pm$0.20 dB,

however, the values does not follow the dissolved oxygen as well as in the case of attenuation. During the second period of higher oxygen production, the amplitude of the first receiver increase in approximately ± 0.15 dB, however, shows an instantaneous decrease near that instant.

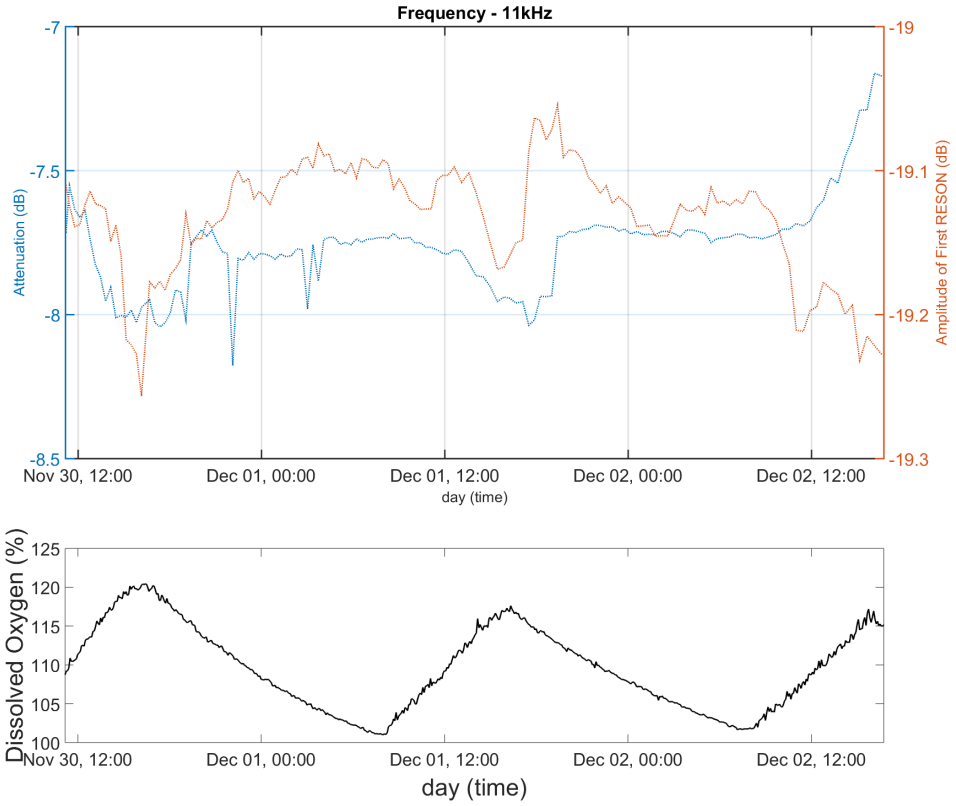

Figure 5.21: At the top, the comparison of the signal attenuation between two receivers (blue) and the amplitude of the signal received by the first receiver, closer to the source (red), for signals transmitted at 11 kHz. At the bottom, the oxygen dissolved during the experiment period (black).

At 11 kHz, as shown in Figure 5.21, the attenuation of the signal increase in about 0.5 dB during the first peak of dissolved oxygen to values close to 8 dB and during the first period of the night the values of attenuation is 7.7 dB, approximately. In the second period with more intensity of sunlight, the attenuation of the signal has increased 0.3 dB to a total of 8 dB. On the other hand, the amplitude of the first receiver during the first peak of dissolved oxygen increase only ± 0.13 dB, however, the values does not follow the dissolved oxygen as well as in the case of attenuation in Figure 5.20. Dur-

ing the second period of higher oxygen production, the amplitude of the first receiver increase in approximately ± 0.08 dB.

As shown in the attenuations figures, the attenuation of the signal propagating over the plants is strongly correlated with dissolved oxygen, which clearly suggests, that there was released bubbles during this period, due to photosynthesis of the marine plants. The amplitude of the first receiver is less correlated with dissolved oxygen, because, even if there is an attenuation of the signal, this attenuation is about $^1/_4$ of attenuation of the signal between the two receivers. Although the box with marine plants were placed between the two receivers, it is possible that the bubbles may slightly reach the first receiver, causing this attenuation.

6

Conclusions

This thesis presents the description of the developed measurement system including the tests and the experiments done during the all steps of this work. The system is tested in ponds and tanks, when the weather conditions favours the bubbles formation by photosynthesis.

The results suggest the significant formation of oxygen bubbles during the photosynthesis, particularly in the periods when there is a higher level of solar radiation.

During the calibration system experiments, it was possible to verify propagation delay of the signal and also a signal attenuation when bubbles were released in the tank. In the final setup experiment, when the stainless steel structure was used to place the hydrophones, both the delay and the attenuation of the signals were verified quite

well. The sound speed decreased, at all frequencies used (4-20 kHz), in approximately 140 m/s. The attenuation of the signal, when the bubbles are released between the receivers, increases between approximately 10 and 22 dB, depending on the frequency. This fact concludes that the system is able to quantify the bubbles production in the water column.

The preliminary experiments conducted show that during high O_2 saturation level the acoustic noise is highly attenuated, probably due to the existence of bubbles. Also shows that in lower productivity conditions the signature of the photosynthetic activity is weak, but, even so, noise power variability correlated with dissolved O_2 measurements is evident for noise components above 2 kHz. In the lower frequencies the variability of the noise power is directly correlated with the water depth. During the experiment shown in section , undersaturation conditions were observed, which may suggest that even under these conditions the photosynthesis presents a signature (change of attenuation) in acoustic data, what may be ascribed to air in plants aerenchyma.

The experiments performed using the developed measurement system were extremely important to better understand how to proceed in the future to estimate bubble production by marine plants. With these experiments it is possible to conclude that solar irradiance is the most relevant parameter for the photosynthesis activity of the marine plants, and therefore, when there is a higher level of sunlight there is a consequent higher production of oxygen. When the water column becomes saturated (O_2 concentration level of O_2 greater than 100%) there is formation and release of oxygen in the form of a bubble. Therefore, as this experiment was carried out in the winter, there was no large bubble production compared to the summer production. However, the small amount of bubbles produced by transplanted plants was verified by acoustic backscatter system. It was possible to verify the attenuation caused by the small amount of bubbles. This attenuation of the signal has peaks during the period of the day which allows to conclude that it is due to the presence of the bubbles. A fact

supporting this theory is that the signal level of the first receiver (there are no plants between the first receiver and the transmitter) despite having a small attenuation, that attenuation is about 4x less than the attenuation between the receivers.

6.1 Future work

As it was demonstrated by the results of the experiments, the measurement system to estimate bubble production by marine plants has a long way to go, until is considered ready to do this estimation. There are several details that need to be addressed to solve some small problems. Although, at this stage, the system needs to be tested in various marine environments with higher levels of bubble production.

So the main objective of the future work is to planning and execution of sea trials, in *Ria Formosa* with the purpose of continuing the study of the quantification of oxygen bubbles production in various environments with marine plants.

Another interesting experiment test would be to repeat the experiment with plants transplanted to a tank, such as the last experiment, but with higher plant density at the bottom of the tank and with other different marine plant species. The aim of this higher density of plants is to increase the level of oxygen concentration in the tank, and in turn, increase the production of bubbles. This experiment would have to be carried out at a time when there is a higher rate of photosynthesis by the plants in order to increase the production of oxygen, that is, preferably would have to be carried out in the summer.

An experiment using the natural production of bubbles by plants has its advantages and disadvantages. We stayed dependent on the production or not of the plants, but the bubbles produced by the plants have the desired size. In other hand, known systems for generating oxygen in a controlled manner are very complicated, i.e., exist but the bubbles formed are huge and the flow is difficult to control. As the bubbles of these systems are large, a possible alternative would be to decrease the frequency

of the signal, however, at low frequencies the measurement system equipment is no longer ideal.

To finish, one last interesting experiment would be to put the whole system with the stainless steel structure inside the tank (C), because in this tank there is a large quantity and density of marine plants of various species. Moreover, in this tank there is also the acoustic noise of the pumps, and it would be quite interesting to estimate bubbles in this environment.

6.2 Publications

During the time of the master's degree, several works were published, with a total of four articles for international conferences.

The following list enumerates the published articles:

- **João Pedro Santos Parente da Silva** (2016) ***Métodos acústicos de caracterização das bolhas produzidas por plantas marinhas***, Jornadas do Mar 2016 – "Novos rumos, novos desafios", 8-11 Novembro 2016, Escola Naval de Lisboa.

- P. Felisberto, **J.P. Silva**, A.J. Silva, S.M. Jesus, C.B. de los Santos, I. Olivé, R. Santos, H. Quental-Ferreira, P. Pousão-Ferreira, M.E. Cunha (2017) ***Acoustic detection of bubbles in a pond covered by the seagrass Cymodocea nodosa***, accepted for Oceans'17 MTS/IEEE conference, Aberdeen, Scotland.

- P. Felisberto, O.C. Rodríguez, **J.P. Silva**, S. Jesus, H. Quental-Ferreira, P. Pousão-Ferreira, M. Cunha, C.B. de los Santos, I. Olivé, R. Santos (2017) ***Monitoring bubble production in a seagrass meadow using a source of oportunity***, in Proc. of Meetings on Acoustics (POMA), Acoustical Society of America, July. DOI: https://doi.org/10.1121/2.0000584

- **J.P. Silva**, D. Nunes, P. Santos, P. Felisberto and A.J. Silva (2017) ***Development of***

a measurement system for assessment of bubble production of seagrass, in Proc. of Int. Congress on Engineering and Sustainability in the XXI Century, 11-13 October, Faro, Portugal.

- P. Felisberto, **J.P. Silva**, A.J. Silva, R. Santos and S.M. Jesus (2018) ***Background noise in areas covered by marine plants in the Ria Formosa lagoon during the summer***, accepted for Oceans'2018 MTS/IEEE/OES conference, Kobe, Japan.

A

User Manual to Connect Red Pitaya

A.1 Connect to SCPI server and Matlab script

The most common and recommended way to connect and use the Red Pitaya STEMLab board is through LAN network. Your LAN network needs to have DHCP settings enabled, which is the case on most local networks. With this, only a simple plug-and-play approach is required. After that, simply follow these 3 simple steps:

1. Connect Red Pitaya board to the router;
2. Connect power supply to the Red Pitaya board;

3. Open your web browser and in the URL filed type **rp-xxxxxx.local/**.

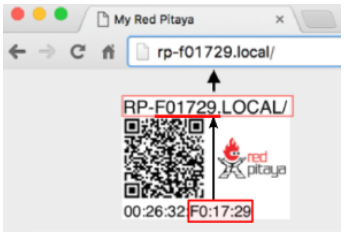

Figure A.1: The xxxxxx are the last 6 characters from MAC address of RedPitaya board. MAC address is written on the Ethernet connector.

After the **third step**, you will get a Red Pitaya board main page and you can access all applications that you have on your board.

Red Pitaya board can be controlled remotely over LAN or wireless interface using Matlab, Labview, Scilab or Python via Red Pitaya SCPI (Standard Commands for Programmable Instrumentation) list of commands connecting the SCPI server.

The connection to the SCPI server is done simply by clicking the SCPI server icon and starting the SCPI server. When SCPI server is started the IP of your board will be shown. This IP you need to input in to your scripts.

1. First, in main page go to **Development** $\Rightarrow$ **SCPI server**

Figure A.2: Example of console of the redpitaya. Main menu at the top and submenu Development below.

2. Start SCPI server by selecting **RUN** button.

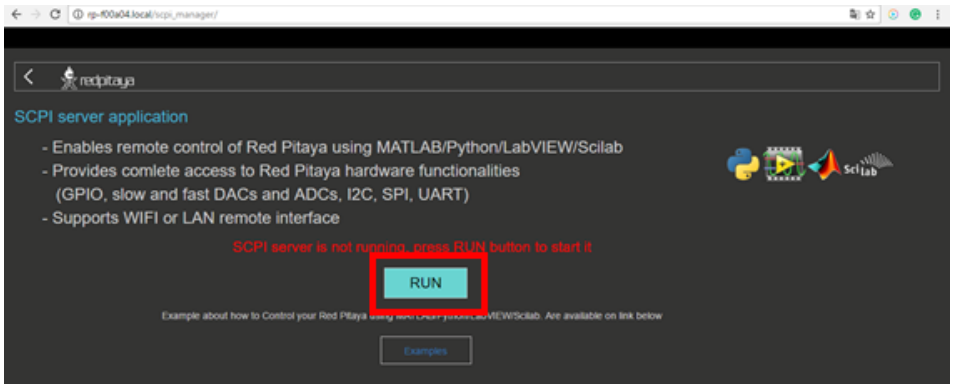

Figure A.3: Example of console of the redpitaya. SCPI server menu.

3. SCPI server is already running. The IP that is shown is the necessary IP to input in to your scripts.

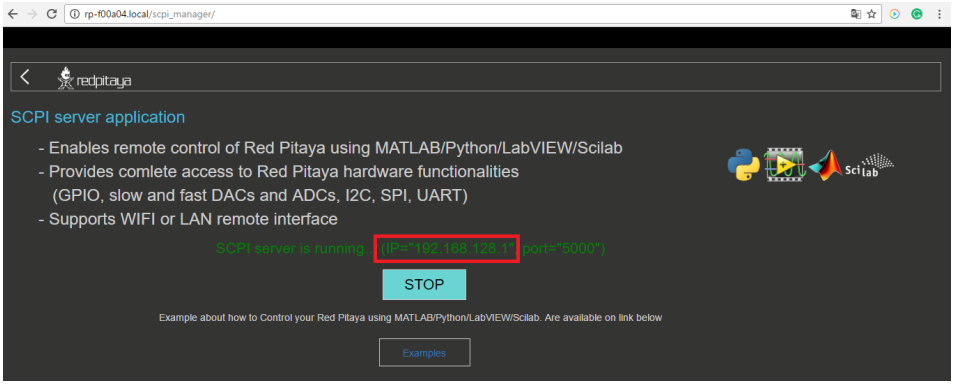

Figure A.4: Example of console of the redpitaya. SCPI server menu after press RUN.

After starting the SCPI server, to connect with the Red Pitaya through a Matlab script with SCPI commands, it is necessary to put in the initialization of the script the IP address of the board and the port, which are shown on the page of figure A.4, and make the connection with Red Pitaya board. An example of an initialization of a script is as follows.

```
%% Define Red Pitaya as TCP/IP object

IP= '192.168.178.56';          % Input IP of your Red Pitaya...
port = 5000;
tcpipObj=tcpip(IP, port);

%% Open connection with your Red Pitaya

fopen(tcpipObj);
tcpipObj.Terminator = 'CR/LF';
```

Figure A.5: An example of initialization Matlab script to connect to Red Pitaya board.

References

Aquariums, N. (2007). Botany-how plants work. http://naturalaquariums.com/plantedtank/0702.html. Retrieved: Nov, 2016.

Au, W. W. & Hastings, M. C. (2008). Principles of marine bioacoustics.

Barber, B. (2014). The effect of temperature on the rate of photosynthesis. https://sciencing.com/effect-temperature-rate-photosynthesis-19595.html. Retrieved: Out, 2016.

Borum, J., Sand-Jensen, K., Binzer, T., Pedersen, O., & Greve, T. M. (2006). *Oxygen Movement in Seagrasses*, (pp. 255–270). Springer.

Brekhovskikh, L. & Lysanov, Y. (2003). Chapter 11 - scattering and absorption of sound by gas bubbles in water. In *Fundamentals of Ocean Acoustics* (pp. 250 – 264). New York: Springer-Verlag.

Felisberto, P., Jesus, S., Zabel, F., Santos, R., Silva, J., Gobert, S., Beer, S., Bjork, M., Mazzuca, S., Procaccini, G., Runcie, J. W., Champenois, W., & Borges, A. V. (2015). Acoustic monitoring of O2 production of a seagrass meadow. *Journal of Experimental Marine Biology and Ecology*, 464(0), 75 – 87.

Felisberto, P., Rodríguez, O., Silva, J., Jesus, A., Quental-Ferreira, H., Pousão-Ferreira, P., Cunha, M., de los Santos, C., Olivé, I., & Santos, R. (2017a). Monitoring buble production in a seagrass meadow using a source of oportunity.

Felisberto, P., Silva, J., Silva, A., Jesus, A., Olivé, I., Santos, R., Quental-Ferreira, H., Pousão-Ferreira, P., & Cunha, M. (2017b). Acoustic detection of bubbles in a pond covered by the seagrass cymodocea nodosa.

Fondriest Environmental, I. (2014). "solar radiation and photosynethically active radiation." fundamentals of environmental measurements. http://www.fondriest.com/environmental-measurements/parameters/weather/photosynthetically-active-radiation/. Retrieved: Nov, 2016.

Lamarre, E. & Melville, W. K. (1995). Instrumentation for the measurement of sound speed near the ocean surface. *Journal of Atmospheric and Oceanic Technology*, 12(2), 317–329.

Medwin, H. & Clay, C. S. (1998). Chapter 8 - bubbles. In H. Medwin & C. S. Clay (Eds.), *Fundamentals of Acoustical Oceanography* (pp. 287 – 347). San Diego: Academic Press.

Netting, R. (2007). Visible light waves. https://science.hq.nasa.gov/kids/imagers/ems/visible.html. Retrieved: Nov, 2016.

Oceanic, N. & Administration, A. (2013). How far does light travel in the ocean? https://oceanservice.noaa.gov/facts/light_travel.html. Retrieved: Out., 2016.

Okeanos aquascaping (2013). Pro-pearling: How to maximize bubble volume in your aquarium. http://www.okeanosgroup.com/blog/aquariums/pro-pearling-how-to-maximize-bubble-volume-in-your-aquarium/. Retrieved: Set., 2016.

Royal Society of Chemistry (2012). Rate of photosynthesis: limiting factors. http://www.rsc.org/learn-chemistry/content/filerepository/CMP/00/001/068/Rate%20of%20photosynthesis%20limiting%20factors.pdf. Retrieved: Oct, 2016.

Scales, H. (2009). How does photosynthesis work underwater? https://www.thenakedscientists.com/articles/questions/how-does-photosynthesis-work-underwater. Retrieved: Out., 2016.

Silverstein, A. (2008). *Photosynthesis.*

StemLab, R. (2016). Remote control (matlab, labview, scilab or python). http://redpitaya.readthedocs.io/en/latest/appsFeatures/remoteControl/remoteControl.html#matlab. Retrieved: Dez, 2016.

Television, N. H. P. (2014). Ocean zones - natureworks. http://www.nhptv.org/natureworks/nwep6c.htm. Retrieved: Nov, 2016.

Terrill, E. J. & Melville, W. K. (2000). A broadband acoustic technique for measuring bubble size distributions: Laboratory and shallow water measurements. *Journal of Atmospheric and Oceanic Technology*, 17(2), 220–239.

Todar, K. (2012). Diversity of microbial metabolism. http://textbookofbacteriology.net/metabolism_6.html. Retrieved: Out., 2016.

Vagle, S. & Farmer, D. M. (1998). A comparison of four methods for bubble size and void fraction measurements. *IEEE journal of oceanic engineering*, 23(3), 211–222.

Watt, M. K. (2000). *A hydrologic primer for New Jersey watershed management*. Technical report, US Geological Survey.

Wetzel, R. G. (2001). *Limnology: lake and river ecosystems*. Gulf Professional Publishing.

Wilson, P. S. & Dunton, K. H. (2009). Laboratory investigation of the acoustic response of seagrass tissue in the frequency band 0.5–2.5 khz. *The Journal of the Acoustical Society of America*, 125(4), 1951–1959.